Master's Thesis

# CHEMICAL PROBES FOR PROTEIN HISTIDINE PHOSPHATASES

Yigun Choi

Department of Chemistry

Graduate School of UNIST

2018

# CHEMICAL PROBES FOR PROTEIN HISTIDINE PHOSPHATASES

Yigun Choi

Department of Chemistry

Graduate School of UNIST

# Chemical Probes for Protein Histidine Phosphatases

A thesis/dissertation
submitted to the Graduate School of UNIST
in partial fulfillment of the
requirements for the degree of
Master of Science

Yigun Choi

06/07/2018 of submission
Approved by

_____

Advisor
Assistant Professor Jung-Min Kee

# Chemical Probes for Protein Histidine Phosphatases

Yigun Choi

This certifies that the thesis/dissertation of Yigun Choi is approved.

06/07/2018

signature

_____

Advisor: Assistant Professor Jung-Min Kee

signature

_____

Associate Professor Jeong Kon Seo

signature

_____

Associate Professor Tae-Hyuk Kwon

# Abstract

Protein phosphorylation is an important class of protein post-translational modifications (PTMs), and it is known to occur on a variety of amino acid side chains including Ser, Thr, Tyr, as well as His, Lys, Arg, Asp, Cys, and Glu. Among them, protein histidine phosphorylation has been implicated in diverse physiological phenomena, including cell signaling, metabolic processes, and immune responses. Even it has been linked to cancer metastasis and diabetes, but further studies have been stalled due to the technical difficulty stemming from the acid lability of phosphohistidine (pHis). To overcome this, I have studied chemical tool for studying protein histidine phosphorylation, especially pHis phosphatase assays.

In chapter I, I reviewed chemical biology of protein histidine phosphorylation, specifically about protein histidine phosphatases. Among them, I mainly focused on phosphohistidine phosphatase 1 (PHPT1), one of the few characterized mammalian pHis-specific protein phosphatases, including its discovery, structure, and biological functions. I also described current methods for studying protein histidine phosphorylation and their limitations.

In chapter II, I introduced two types of fluorescent probes for protein histidine phosphatases, including their design, synthesis, validation, and optimization. To our delight, our probes showed meaningful fluorescence decrease upon dephosphorylation by PHPT1, thereby facilitating real-time measurement of PHPT1 activity. In particular, our probes were only sensitive to PHPT1, showing no activity to other known protein histidine phosphatases. With these probes in hand, the kinetic parameters of PHPT1 was conveniently obtained, showing orders of magnitude difference from the literature values. This result demonstrated the limitation of previous methods for enzyme kinetics and the potential values of our novel PHPT1 probes.

# Table of Contents

# Chapter I. Introduction to Protein Histidine Phosphorylation

## 1.1. Protein phosphorylation

Protein phosphorylation is the most prevalent post-translational modifications (PTMs) which occur on proteins after translation by ribosomes, usually catalyzed by enzymes. According to the statistics of PTMs, phosphorylation accounts for ~65% of total experimentally observed PTMs.[1] Among the twenty proteinogenic amino acids, nine are known to be phosphorylated: serine (Ser), threonine (Thr), tyrosine (Tyr), histidine (His), lysine (Lys), arginine (Arg), aspartate (Asp), glutamate (Glu), and cysteine (Cys). Historically, studies on protein phosphorylation have mainly concentrated on Ser, Thr, and Tyr, and consequently revealed their crucial roles in cellular metabolism and signal transduction pathways. Extensive research on Tyr phosphorylation was culminated by the development of imatinib (marketed as Gleevec®), a tyrosine kinase inhibitor, as a blockbuster drug for chronic myelogenous leukemia and acute lymphocytic leukemia.

Ser, Thr, and Tyr have hydroxyl groups which are phosphorylated to form stable phosphoesters, called protein *O*-phosphorylation. Unlike this, protein *N*-phosphorylation on His and Arg side chains to form phosphoramidates has not been studied as extensively due to their chemical instability, particularly under acidic conditions. However, it does not necessarily mean that protein *O*-phosphorylation is more important than protein *N*-phosphorylation. For example, pHis is best known as a key intermediate of two-component systems (TCS) in bacteria, fungi, and plant[2]. Phosphoarginine (pArg) has recently been reported as a protein degradation marker in prokaryotes, similar to the role of ubiquitin in eukaryotes.[3] Both pHis and pArg are main research targets in our laboratory, but this thesis will focus on pHis.

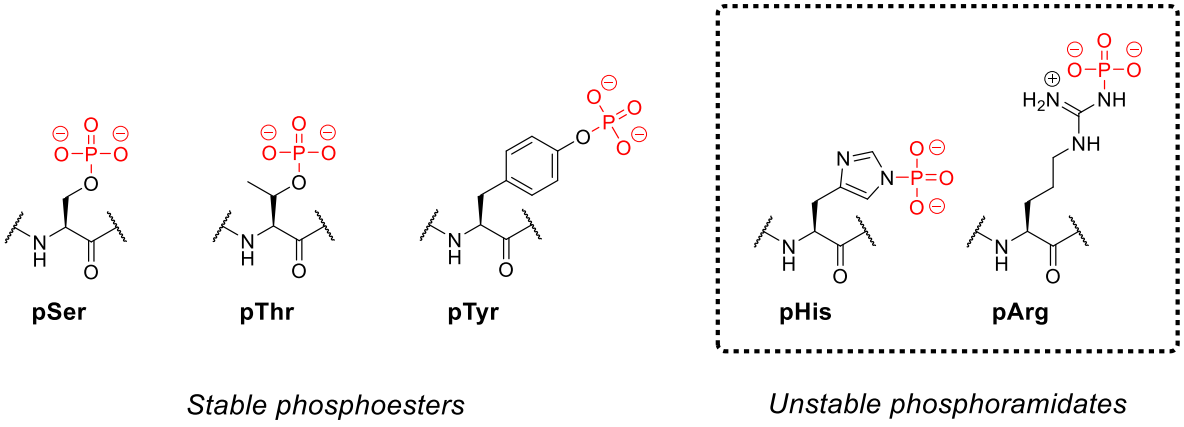


**Figure 1. Structures of representative phosphoamino acids.**

## 1.2. Protein histidine phosphorylation

### *1.2.1. Biochemistry of phosphohistidine*

The unique characteristic of pHis compared to other phosphoamino acids is that it can exist as two isomeric forms, τ(tele)-phosphohistidine (τ-pHis) and π(pros)-phosphohistidine (π-pHis). τ- and π-pHis are also called 3- and 1-pHis because their phosphorylated positions are N3 and N1 of imidazole ring, respectively. Both pHis isomers are found in biological systems. Of the two, τ-pHis is thermodynamically more favorable compared to π-pHis, the kinetic product which can even isomerize to τ-pHis.[4] While diphosphohistidine can be chemically synthesized, it has not been detected in proteins yet.[5]

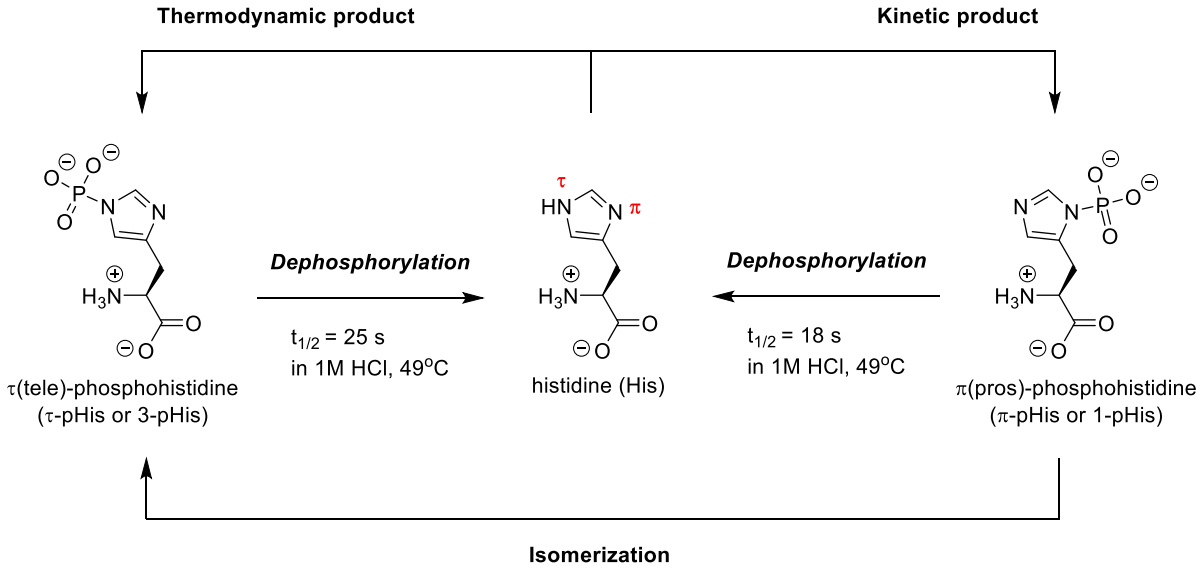


**Figure 2. Structures and chemistry of pHis isomers.[6]**

The phosphoramidate in pHis is more thermodynamically unstable (ΔG° of hydrolysis = -12 to -14 kcal/mol) than phosphoester in pSer (ΔG° of hydrolysis = -6.5 kcal/mol) or pTyr (ΔG° of hydrolysis = -6.5 kcal/mol).[7] This instability arises from poor orbital overlap between nitrogen lone pair and phosphorous d-orbital which is in a higher energy shell and therefore less involved in the conjugation effect.[8] Moreover, electronegativity of nitrogen is lower than oxygen, hence it makes the imidazole in pHis a better leaving group by *N*-protonation ($pK_a$ = 6.4) while phosphoester is poorly protonated ($pK_a$ < 0).[9]

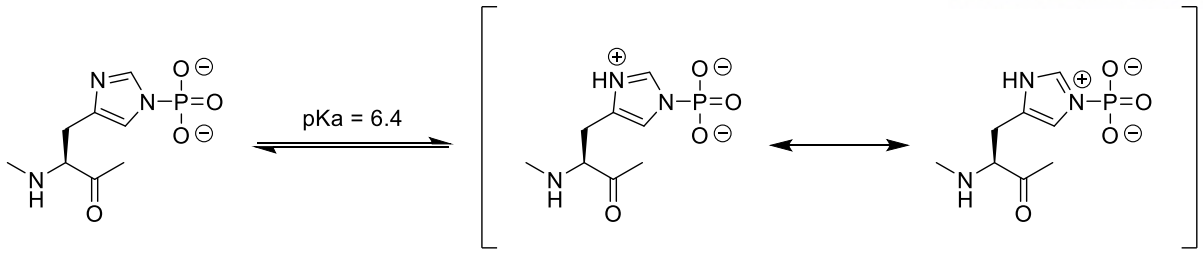


**Figure 3. Acid-base equilibrium and resonance of pHis.**

### *1.2.2. Biological functions of protein histidine phosphorylation*

Although protein histidine phosphorylation is less explored because of the technical difficulties in research, several biological functions of pHis have been reported. Among them, the best-known one is the two-component system (TCS), a key signal transduction pathway in bacteria, fungi, or plants.[10] TCS consists of a histidine kinase (HK) and a response regulator (RR). When HK is activated by environmental stimuli, it is autophosphorylated on its histidine residue, and subsequently transfer the high-energy phosphoryl group to an aspartate (Asp) residue of its cognate RR. Phosphorylation of the Asp results in the conformational change of the RR and subsequent binding to DNA as a transcription factor (TF).

Due to the facile phosphoryl group transfer of pHis, several proteins are known to have pHis as enzyme intermediates. For example, the phosphoryl group on pHis11 of phosphoglycerate mutase 1 (PGAM1) is transferred to 3-phosphoglycerate (3-PG) to form 2,3-bisphosphoglycerate (2,3-BPG), and the 3-phosphoryl group of 2,3-BPG is subsequently returned to His11 of PGAM1 to yield 2-phosphoglycerage (2-PG) as the product.[11] With similar phosphoryl transfer mechanisms, pHis intermediates are also found in other enzymes such as ATP-citrate lyase (ACLY)[12], glucose-6-phosphatase (G3Pase)[13], and succinyl-CoA synthetase (SCS)[14]. Notably, the last one is the first example of pHis, identified in 1962.[15]

pHis is found not only as enzymatic intermediates but also as the phosphorylation product by protein histidine kinases. For example, isoforms of nuclear diphosphate kinase (NDPK)[16], the only fully-characterized mammalian histidine kinases, phosphorylate the epithelial calcium channel TRPV5[17] and the calcium-activated potassium channel KCa3.1[18]. NDPK is also involved in G protein signaling by phosphorylation of the $\beta$-subunit of heterotrimeric G proteins.[19] All of the above examples of histidine phosphorylation by NDPK are known be dephosphorylated by phosphohistidine phosphatase 1 (PHPT1), so details about PHPT1 will be described later in 1.2.3.1. Another example is histone H4 histidine phosphorylation by histone H4 histidine kinase (HHK).[20] It is presumably related to chromatin regulation, but the identify HHK is still unclear.[21]

### *1.2.3. Protein histidine phosphatases*

#### *1.2.3.1. Phosphohistidine phosphatase 1*

PHPT1 is the first mammalian pHis phosphatase discovered by Ek and coworkers in 2002.[22] In this work, the authors used a pHis-containing peptide Suc-Ala-pHis-Pro-Phe-pNA to probe the pHis phosphatase activity in porcine liver cytosol with the malachite green assay (described in 1.3.3). They observed the phosphatase activity which was not inhibited by okadaic acid or ethylene diamine tetraacetic acid (EDTA). Finally, a 14 kDa protein of 125 amino acids was cloned from human cDNA library, and it was found to be specific to pHis while inactive towards pSer, pThr, and pTyr.

Coincidentally, this protein was independently discovered by Klumpp and coworkers in the same year, named as protein histidine phosphatase (PHP).[23] In this work, the authors used chemotaxis protein A (CheA) whose His48 was labeled with [γ-$^{32}$P]ATP as the substrate. Dephosphorylation of [$^{32}$P-His]CheA was observed in homogenates of heart, kidney, and liver of a rabbit, and subsequently PHPT1 was purified from soluble extracts of rabbit liver. They also verified the specificity of PHPT1 to pHis among phosphoamino acids.

To date, PHPT1 has been reasonably well characterized, and even its 3D structures were reported. The first crystal structure was determined by Busam and coworkers in 2006,[24] with a resolution of 1.9 Å using multi-wavelength anomalous dispersion (MAD). In this study, His53 was defined as a key residue in the active site, and its mutation to alanine (Ala) led to complete loss of the catalytic activity. In 2009, another 3D structure of PHPT1 was reported by Gong and coworkers using nuclear magnetic resonance (NMR) spectroscopy. They also determined the active site of PHPT1 by mutagenesis study, which is different from previously reported one. In this study, the catalytic mechanism of PHPT1 was proposed that His53 acts as a general base, activating a water molecule to attack the phosphoryl group of pHis under the stabilization of the transition state by positive charge of Lys21.

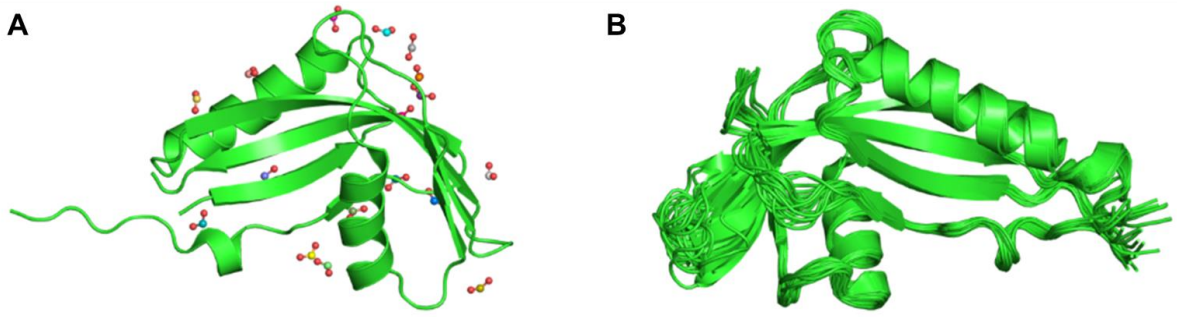


**Figure 4. Three-dimensional (3D) structures of PHPT1. (A) Crystal structure by X-ray, image from PDB 2hw4. (B) Solution structure by NMR, image from PDB 2ai6.**

Despite the above studies, the biological functions of PHPT1 were not completely understood. PHPT1 is known to catalyze the dephosphorylation of proteins which are phosphorylated by NDPK, as previously described in 1.2.2. NDPK is encoded by nm23, a metastasis suppressor gene, also known as NME.[25] Accordingly, PHPT1 may be related to tumor metastasis because it can reverse the histidine kinase reaction by NDPK. In 2010, a role of PHPT1 in human lung cancer was first reported by Xu and coworkers.[26] They observed higher expression of PHPT1 in highly metastatic human lung cancer cell line CL1-5 when compared to poorly metastatic CL1-0. They also observed significant decrease of cell migration and invasion in PHPT1-knocked down CL1-5. In addition, PHPT1-overexpressing human lung cancer cell line H1299 showed higher cell migration and invasion rate. While the expression level of PHPT1 did not affect cell proliferation, its potential role in cell migration and invasion was proposed. Subsequently in 2016, it was reported that the lung cancer suppression by knockdown of PHPT1 was through the regulation of nuclear factor kappa-light-chain-enhancer of activated B cells (NF-κB) signaling pathway. Similarly, PHPT1 was also reported to be related to renal cancer in 2015.[27]

Carrying out the reverse roles of NDPK, PHPT1 dephosphorylates the active site pHis780 of ATP-citrate lyase (ACL) in pancreatic β-cells, implicating its role in insulin secretion.[28] In addition, PHPT1 inhibits the ion channel KCa3.1 by dephosphorylation of pHis358, which is conversely activated by NDPK-B, thereby negatively regulating CD4 T cells.[29] Even more interestingly, PHPT1 was recently proposed as a regulator of the epidermal growth factor receptor (EGFR), a transmembrane protein which plays a role as a signal transducer to control diverse cellular processes.[30] Upregulation of EGFR has been strongly linked to various cancers[31], so if a definite relationship between PHPT1 and EGFR is revealed, it will have significant impact on oncogene research.

#### *1.2.3.2. Enzymes with pHis phosphatase activities*

Besides PHPT1, there are several phosphatases which have phosphatase activities for pHis: phosphohistidine phosphatase SixA, phospholysine phosphohistidine inorganic pyrophosphate phosphatase (LHPP), phosphoglycerate mutase 5 (PGAM5), protein phosphatase 1, 2A, and 2C (PP1, PP2A, and PP2C).

SixA is the first reported bacterial pHis phosphatase which is implicated in TCS.[32] It has phosphatase activity towards histidine-containing phosphotransfer (HPt) domain of aerobic respiration control sensor protein ArcB (a histidine kinase). Thereby, SixA plays an important role of *Escherichia coli (E. coli)* anaerobiosis by modulating His-to-Asp phosphorelay signal transduction.[33] Interestingly, SixA has been reported to specific to ArcB, being inactive to other pHis substrates.

LHPP was first known as a 56 kDa inorganic pyrophosphatase, purified from bovine liver in

1997.[34] In the next year, its phosphatase activity towards free τ-pHis and pLys was confirmed *in vitro*.[35] However, no specific biological substrates of LHPP have been identified up to recently.[36] In 2018, Hindupur and coworkers revealed nine potential protein targets of LHPP, including ATP citrate lyase, chromagranin A, and histone H2A.V.[37] More significantly, they identified LHPP as a tumor suppressor protein in liver cancer. LHPP has also been regarded as a key risk factor for depressive disorder[38] and testicular germ cell tumor[39], so its biological importance in cancer research has been increasingly recognized.

PGAM5 is an enzyme that converts 3-PG to 2-PG in glycolysis[40], and also known as a protein Ser/Thr phosphatase.[41] Lately, it was identified as a mammalian pHis phosphatase that specifically dephosphorylates NDPK-B.[42] When the phosphorylation on His118 of NDPK-B is inhibited by PGAM5, phosphorylation on His358 of KCa3.1 is sequentially inhibited to deactivate this ion channel activity, thereby regulating proinflammatory cytokine production in T helper cells.

In addition to these phosphatases, PP1, PP2A, and PP2C, originally known as protein Ser/Thr phosphatases, were also reported to dephosphorylate pHis in histone H4 protein *in vitro*.[43] Kim and coworkers reported this observation in 1993, making it the first reported case of protein histidine phosphatase activity in mammals. However, it is still unclear whether pHis proteins are their cognate substrates *in vivo*.

## 1.3. Research tools for studying protein histidine phosphatases

### *1.3.1. $^{32}$P-Radiolabeling*

The most traditional method for studying protein phosphorylation is $^{32}$P-isotopic labeling on phosphorylated amino acid residues. The protein substrate and its kinase are incubated with [γ-$^{32}$P]ATP, then phosphorylated sites are labeled by $^{32}$P. This $^{32}$P-labeled phosphoprotein can be analyzed for the quantification of phosphorylation by phosphorimaging or scintillation counting. In fact, Klumpp and coworkers discovered PHPT1 using $^{32}$P-labeled CheA (refer to section 1.2.3.1).

This method is very sensitive to the recognition of existence or nonexistence of phosphorylated protein. However, the most significant limitation is that it is not specific towards any specific type of protein phosphorylation. Simply, pHis cannot be distinguished from other phosphoamino acids like pLys. Therefore, phosphoamino acid analysis should be accompanied to identify what specific amino acid is phosphorylated.[44] For example, when a mixture of $^{32}$P-labeled phosphoproteins is treated by a base, remaining phosphoamino acids should be pHis, pLys, or pTyr which are stable in basic conditions. Among these three phosphoamino acids, only pTyr will survive an acid treatment, so disappeared bands can be assumed as pHis or pLys. Even with this laborious method, specific identification of pHis is very

challenging. Moreover, radiolabeling is difficult to do experiment because it needs special facilities to treat a radioisotope.

### *1.3.2. para-Nitrophenylphosphate (pNPP)*

pNPP is a chromogenic substrate firstly used for alkaline phosphatases.[45] Phosphoryl group of pNPP is hydrolyzed to yield a free phosphate and *para*-nitrophenol (pNP). Under slightly basic condition, pNP exists as a phenolate form (p$K_a$ = 7.2) and it absorbs 405 nm wavelength to release yellow color, which can be easily quantified by the absorbance at 405 nm.

pNPP assay can be applied to various phosphatases including acid phosphatase[46] and protein tyrosine phosphatase (PTP).[47] Also, it was used as a substrate for PHPT1 to observe the impact of oxidative modification on the enzyme activity.[48] However, pNPP is not pHis-based substrates because its structure is based on aryl phosphate and therefore not suitable for determining the accurate kinetics parameters of actual pHis substrates. Similarly, 6,8-difluoromethylumbelliferyl phosphate (DiFMUP) was used as a fluorogenic substrate for PHPT1 assay.[49] It was much more improved than pNPP in terms of the sensitivity and enzyme turnover, but still have the same limitation that it is not pHis-based substrate Therefore, it cannot be specific towards pHis phosphatases.

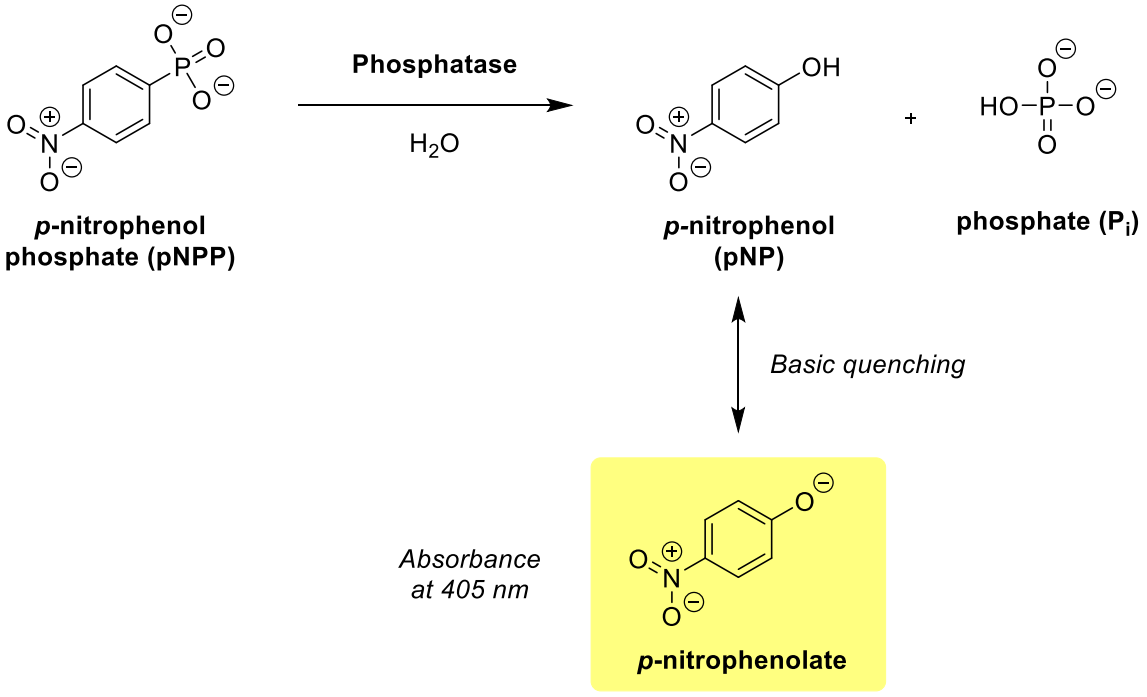


**Figure 5. Principle of pNPP phosphatase assays.**

### *1.3.3. Malachite green*

Malachite green is an organic dye used for detection of inorganic phosphate.[50] When a free phosphate is liberated from phosphorylated protein substrate by a phosphatase, it forms a polymerized complex with ammonium molybdate in acidic condition. Then, malachite green is added to finally form a malachite green phosphomolybdate complex which absorbs 620-640 nm wavelength to release green color. This method is suitable for detection and quantification of free phosphate, but it cannot be used for real-time observation of enzyme kinetics because it has to hydrolyze phosphate to detect signals. When Ek and coworkers first identified PHPT1 in 2002, malachite green was used in the phosphatase assay (refer to section 1.2.3.1).

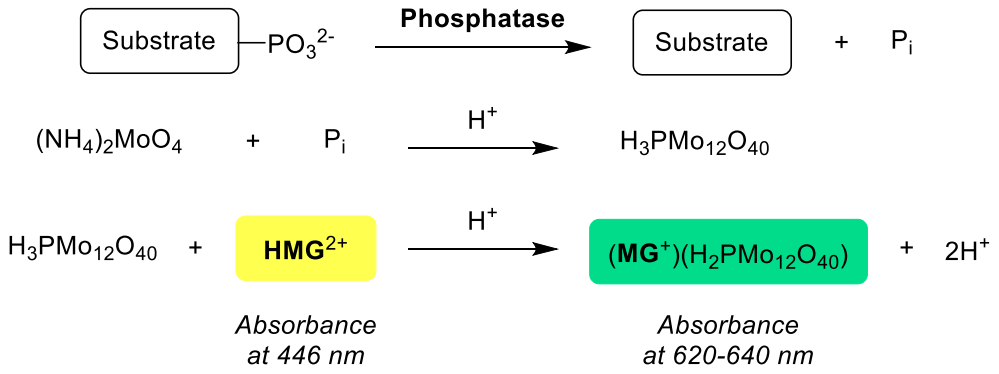


**Figure 6. Mechanism of malachite green phosphatase assay.**

### *1.3.4. $^1$H-NMR*

NMR measurement can also be for studying protein histidine phosphatases. There are two proton NMR peaks of the imidazole ring in a histidine residue, and their chemical shifts are shifted upon phosphorylation. Thus, His and pHis can be distinguished by their $^1$H chemical shifts. This method provides the most accurate in quantitative information about pHis dephosphorylation because it can quantify both pHis and His with the integration values of NMR peaks. In 2010, Attwood and coworkers determined the kinetic parameters of PHPT1 using NMR spectroscopy.[51] However, this method is rather limited because the time for NMR measurement including shimming and locking should be considered, hence the time intervals in enzyme kinetic studies cannot be shortened. Furthermore, NMR measurement needs relatively large amount of peptide or protein substrates. In the case of Attwood's work, about 5 mM of histone H4 peptide was used and the full-length histone H4 could not be used due to its insufficient solubility.

### *1.3.5. pHis-specific antibody*

The latest research tool for studying pHis is the pHis-specific antibody. Antibodies are valuable because they can be utilized in enzyme-linked immunosorbent assay (ELISA) or western blot for detection and quantification of protein phosphorylation and immunoprecipitation (IP) for isolation and enrichment of phosphorylated proteins from biological samples. Despite the value, pHis-specific antibody had not been developed until 2000s due to the chemical instability of pHis.

In 2010, Kee and coworkers developed stable pHis analogue phosphoryl-triazolyl alanine (pTza), and obtained the first pHis-specific antibody using pTza as the hapten.[52] This antibody was specific to pHis18 in the histone H4 tail peptide only, so they subsequently developed the first pan-pHis antibody using another pHis analogue phosphoryl-triazolyl ethylamine (pTze) in 2013.[53] Since it had mild cross-reactivity to pTyr, Kee and coworkers improved the pan-pHis antibody using a second-generation pHis analogue phosphono-pyrazolyl ethylamine (pPye) in 2015.[54] In the same year, Lilley and coworkers developed another second-generation pHis analogue phosphoryl-pyrazolyl alanine (pPza) and resulting pan-pHis antibody.[55] Also in 2015, Fuhs and coworkers developed monoclonal τ- and π-pHis antibodies using pTza isomers introduced by Kee and coworkers.[56]

Of course, pHis-specific antibodies are essential for extensive study of protein histidine phosphorylation. However, ELISA and western blot are not very convenient for the kinetic studies of protein histidine phosphatases because they are time consuming and laborious endpoint assays.

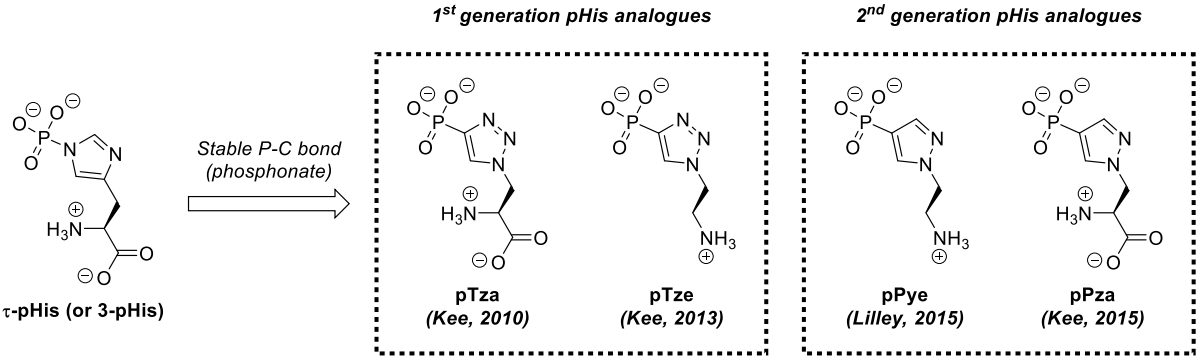


**Figure 7. Structures of stable pHis analogues.**

## 1.4. Conclusion

Protein histidine phosphorylation was first observed more than half a century ago, and its biological functions has been only gradually revealed so far. It plays a central role in the TCS in prokaryotes and lower eukaryotes, epigenetic regulation, and metabolic enzyme intermediates.

To date, seven fully characterized proteins are reported to have protein pHis phosphatase activities

(PHPT1, SixA, LHPP, PGAM5, PP1, PP2A, and PP2C). Among these, PHPT1 has been related to lung and renal cancer as well as G protein signaling and ion channel regulation. In spite of its biological significance, there are no appropriate research tools for kinetic studies for PHPT1 and other pHis-specific phosphatases. In chapter II, I will describe our fluorescent activity probes for studying PHPT1 to address this lack of tools.

**Table 1. List of known pHis-related proteins.**

| Category | Protein | pHis site | Target protein |
|---|---|---|---|
| Kinase | Nucleoside diphosphate kinase A (NDPK-A)[16] | π-pHis118[a] | ACLY, annexin A1 |
| | Nucleoside diphosphate kinase B (NDPK-B)[1616] | π-pHis118[a] | KCa3.1, TRPV5, G protein β-subunit |
| | Histone H4 histidine kinase (HHK)[21,57] | | Histone H4 |
| | Histidine kinase in TCS[10] | | |
| Phosphatase | Phosphohistidine phosphatase 1 (PHPT1)[22,23] | | Substrates of NDPK, histone H4 |
| | Phosphohistidine phosphatase SixA[32] | | ArcB[33] |
| | Phospholysine phosphohistidine inorganic pyrophosphate phosphatase (LHPP)[34] | | Nine proteins[37] (listed below)[b] |
| | Phosphoglycerate mutase 5 (PGAM5)[41] | τ -pHis105 | NDPK-B[42] |
| | Protein phosphatase 1, 2A, and 2C (PP1, PP2A, and PP2C)[43] | | Histone H4 |
| Substrate | Histone H4[20] | pHis18[c], pHis75[c] | |
| | Calcium-activated potassium channel KCa3.1[18] | τ-pHis358 | |
| | Transient receptor potential cation channel subfamily V member 5 (TRPV5)[17] | τ-pHis711 | |
| | Aerobic respiration control sensor protein ArcB[33] | pHis292, pHis717 | |
| | Thymidylate synthase[58] | pHis298 | |
| | Annexin A1[59] | pHis103 | |
| | Heterotrimeric G proteins β-subunit[19] | pHis266 | |
| Enzyme intermediate | Heat shock protein 70 (Hsp70)[60] | τ-pHis89 | |
| | Succinyl-CoA synthetase (SCS)[14] | τ-pHis299 | |
| | ATP-citrate lyase (ACLY)[12] | τ-pHis760 | |
| | Glucose-6-phosphatase (G3Pase)[13] | pHis167 | |
| | Prostatic acid phosphatase (PAP)[61] | τ-pHis | |
| | Phosphoglycerate mutase 1(PGAM1)[62] | τ-pHis11 | |
| | Phospholipase D[63] | pHis94 | |

a) Autophosphorylated site.

b) ACLY, chromagranin A, histone H2A.V, HMGB1, IGFN1, LEO1, MRI1, RPL36A, and septin-2.

c) Both τ- and π-pHis isomers are formed, depending on sources of HHK.[64]

## 1.5. Reference

[1] Khoury, G. A.; Baliban, R. C.; Floudas, C. A. Proteome-wide post-translational modification statistics: Frequency analysis and curation of the swiss-prot database. *Sci. Rep.* **2014**, *1*, 1–5.

[2] Khorchid, A.; Ikura, M. Bacterial histidine kinase as signal sensor and transducer. *Int. J. Biochem. Cell Biol.* **2006**, *38*, 307−312.

[3] Trentini, D. B.; Suskiewicz, M. J.; Deszcz, L.; Mechtler, K. Arginine phosphorylation marks proteins for degradation by the ClpCP protease. *Nature* **2016**, *539*, 48–53.

[4] Hultquist, D. E. The preparation and characterization of phosphorylated derivatives of histidine. *Biochim. Biophys. Acta* **1968**, *153*, 329−340.

[5] Besant, P. G.; Attwood, P. V. Detection and analysis of protein histidine phosphorylation. *Mol. Cell. Biochem.* **2009**, *329*, 93-106.

[6] Kee, J. M.; Muir, T. W. Chasing phosphohistidine, an elusive sibling in the phosphoamino acid family. *ACS Chem. Biol.* **2012**, *7*, 44–51.

[7] Stock, J. B.; Stock, A. M.; Mottonen, J. M. Signal transduction in bacteria. *Nature* **1990**, *344*, 395-400.

[8] Modro, T, A. Phosphoric and carboxylic amides; comparison of bonding and reactivity. *ACS Symposium Series* **1981**, *171*, 619–622.

[9] Hultquist, D. E.; Moyer, R. W.; Boyer, P. D. The preparation and characterization of 1-phosphohistidine and 3-phosphohistidine. *Biochemistry* **1966**, *5*, 322–331.

[10] Stock, A. M.; Robinson, V. L.; Goudreau, P. N. Two-component signal transduction. *Annu. Rev. Biochem.* **2000**, *69*, 183-215.

[11] Britton, H. G.; Clarke, J. B. The mechanism of the phosphoglycerate mutase reaction. *Biochem. J.* **1969**, 112, 10-11.

[12] Walinder, O. Identification of a phosphate-incorporating protein from bovine liver as nucleoside diphosphate kinase and isolation of 1-$^{32}$P-phosphohistidine 3-$^{32}$P-phosphohistidine and N- ε-$^{32}$P-phospholysine from erythrocytic nucleoside diphosphate kinase incubated with adenosine triphosphate-$^{32}$P. *J. Biol. Chem.* **1968**, *243*, 3947− 3952.

[13] Ghosh, A.; Shieh, J.-J.; Pan, C.-J.; Chou, J. Y. Histidine 167 is the phosphate acceptor in glucose-6-phosphatase-β forming a phosphohistidine enzyme intermediate during catalysis. *J. Biol. Chem.* **2004**, *279*, 12479−12483.

[14] Kreil, G., & Boyer, P. D. Detection of bound phosphohistidine in E. coli succinate thiokinase. *Biochem. Biophys. Res. Commun.* **1964**, *16*, 551–555.

[15] Boyer, P. D.; DeLuca, M.; Ebner, K. E.; Hultquist, D. E.; Peter, J. B. Identification of phosphohistidine digests from a probable intermediate of oxidative phosphorylation. *J. Biol. Chem.* **1962**, *237*, 3306-3308.

[16] Attwood, P. V; Muimo, R. The actions of NME1/NDPK-A and NME2/NDPK-B as protein kinases. *Lab. Investig.* **2018**, *98*, 283–290.

[17] Cai, X.; Srivastava, S.; Surindran, S.; Li, Z.; Skolnik, E. Y. Regulation of the epithelial $Ca^{2+}$ channel TRPV5 by reversible histidine phosphorylation mediated by NDPK-B and PHPT1. *Mol. Biol. Cell* **2014**, *25*, 1244–1250.

[18] Srivastava, S.; Li, Z.; Ko, K.; Choudhury, P.; Albaqumi, M.; Johnson, A. K.; Yan, Y.; Backer, J. M.; Unutmaz, D.; Coetzee, W. A.; Skolnik, E. Y. Histidine phosphorylation of the potassium channel KCa3.1 by nucleoside diphosphate kinase B is required for activation of KCa3.1 and CD4 T cells. *Mol. Cell* **2006**, *24*, 665–675.

[19] Cuello, F.; Schulze, R. A.; Heemeyer, F.; Meyer, H. E.; Lutz, S.; Jakobs, K. H.; Niroomand, F.; Wieland, T. Activation of heterotrimeric G proteins by a high energy phosphate transfer via nucleoside diphosphate kinase (NDPK) B and Gβ subunits. *J. Biol. Chem.* **2003**, *278*(9), 7220–7226.

[20] Smith, D. L.; Bruegger, B. B.; Halpern, R. M.; Smith, R. A. New histone kinases in nuclei of rat tissues. *Nature* **1973**. *246*, 103− 104.

[21] Besant, P. G.; Tan, E.; Attwood, P. V. Mammalian protein histidine kinases. *Int. J. Biochem. Cell Biol.* **2003**, *35*, 297–309.

[22] Ek, P.; Pettersson, G.; Ek, B.; Gong, F.; Li, J. P.; Zetterqvist, Ö. Identification and characterization of a mammalian 14-kDa phosphohistidine phosphatase. *Eur. J. Biochem.* **2002**, *269*, 5016–5023.

[23] Klumpp, S.; Hermesmeier, J.; Selke, D.; Baumeister, R.; Kellner, R.; Krieglstein, J. Protein histidine phosphatase: A novel enzyme with potency for neuronal signaling. *J. Cereb. Blood Flow Metab.* **2002**, *22*, 1420–1424.

[24] Busam, R. D.; Thorsell, A. G.; Flores, A.; Hammarström, M.; Persson, C.; Hallberg, B. M. First structure of a eukaryotic phosphohistidine phosphatase. *J. Biol. Chem.* **2006**, *281*, 33830–33834.

[25] Steeg, P. S.; Bevilacqua, G.; Kopper, L.; Thorgeirsson, U. P.; Talmadge, J. E.; Liotta, L. A.; Sobel, M. E. Evidence for a novel gene associated with low tumor metastatic potential. *J. Natl. Cancer Inst.* **1988**, *80*, 200-204.

[26] Xu, A.; Hao, J.; Zhang, Z.; Tian, T.; Jiang, S.; Hao, J., Liu, C.; Huang, L.; Xiao, X.; He, D. 14-kDa phosphohistidine phosphatase and its role in human lung cancer cell migration and invasion. *Lung Cancer* **2010**, *67*, 48–56.

[27] Shen, H.; Yang, P.; Liu, Q.; Tian, Y. Nuclear expression and clinical significance of phosphohistidine phosphatase 1 in clear-cell renal cell carcinoma. *J. Int. Med. Res.* **2015**, *43*, 747–757.

[28] Kamath, V.; Kyathanahalli, C. N.; Jayaram, B.; Syed, I.; Olson, L. K.; Ludwig, K.; Klumpp, S.; Krieglstein, J.; Kowluru, A. Regulation of glucose- and mitochondrial fuel-induced insulin secretion by a cytosolic protein histidine phosphatase in pancreatic β-cells. *Am. J. Physiol. Endocrinol. Metab.* **2010**, *299*, E276–E286.

[29] Srivastava, S.; Zhdanova, O.; Di, L.; Li, Z.; Albaqumi, M.; Wulff, H.; Skolnik, E. Y. Protein histidine phosphatase 1 negatively regulates CD4 T Cells by inhibiting the $K^+$ channel KCa3.1. *Proc. Natl. Acad. Sci. U.S.A.* **2008**, *105*, 14442–14446.

[30] Wernicke, J. Regulation of EGF receptor activation by phosphohistidine phosphatase PHPT1. *PhD Thesis, Technische Universität Dortmund* **2017**.

[31] Yewale, C.; Baradia, D.; Vhora, I.; Patil, S.; Misra, A. Epidermal growth factor receptor targeting in cancer: A review of trends and strategies. *Biomaterials* **2013**, *34*, 8690–8707.

[32] Ogino, T.; Matsubara, M.; Kato, N.; Nakamura, Y.; Mizuno, T. An Escherichia coli protein that exhibits phosphohistidine phosphatase activity towards the HPt domain of the ArcB sensor involved in the multistep His-Asp phosphorelay. *Mol. Microbiol.* **1998**, *27*, 573–585.

[33] Matsubara, M.; Mizuno, T. The SixA phospho-histidine phosphatase modulates the ArcB phosphorelay signal transduction in *Escherichia coli*. *FEBS Lett.* **2000**, *470*, 118–124.

[34] Hiraishi, H.; Ohmagari, T.; Otsuka, Y.; Yokoi, F.; Kumon, A. Purification and characterization of hepatic inorganic pyrophosphatase hydrolyzing imidodiphosphate. *Arch. Biochem. Biophys.* **1997**, *341*, 153–159.

[35] Hiraishi, H.; Yokoi, F.; Kumon, A. 3-phosphohistidine and 6-phospholysine are substrates of a 56-kDa inorganic pyrophosphatase from bovine liver. *Arch. Biochem. Biophys.* **1998**, *349*, 381–387

[36] Fuhs, S. R.; Hunter, T. pHisphorylation: the emergence of histidine phosphorylation as a reversible regulatory modification. *Curr. Opin. Cell Biol.* **2017**, *45*, 8–16.

[37] Hindupur, S. K.; Colombi, M.; Fuhs, S. R.; Matter, M. S.; Guri, Y.; Adam, K.; Cornu, M.; Piscuoglio, S.; Ng, C. K. Y.; Betz, C.; Liko, D.; Quagliata, L.; Moes, S.; Jenoe, P.; Terracciano, L. M.; Heim, M. H.; Hunter, T.; Hall, M. N. The protein histidine phosphatase LHPP is a tumour suppressor. *Nature* **2018**, *555*, 678–682.

[38] CONVERGE consortium. Sparse whole-genome sequencing identifies two loci for major depressive disorder. *Nature* **2015**, *523*, 588–591.

[39] Wang, Z.; McGlynn, K. A.; Rajpert-De Meyts, E.; Bishop, D. T.; Chung, C. C.; Dalgaard, M. D.; Greene, M. H.; Gupta, R.; Grotmol, T.; Haugen, T. B.; Karlsson, R.; Litchfield, K.; Mitra, N.; Nielsen, K.; Pyle, L. C.; Schwartz, S. M.; Thorsson, V.; Vardhanabhuti, S.; Wiklund, F.; Turnbull, C.; Chanock, S. J.; Kanetsky, P. A.; Nathanson, K. L.; Testicular Cancer Consortium. Meta-analysis of five genome-wide association studies identifies multiple new loci associated with testicular germ cell tumor. *Nat. Genet.* **2017**, *49*(7), 1141–1147.

[40] Fothergill-Gilmore, L. A.; Watson, H. C. The phosphoglycerate mutase. *Adv. Enzymol.* **1989**, *62*, 227-313.

[41] Takeda, K.; Komuro, Y.; Hayakawa, T.; Oguchi, H.; Ishida, Y.; Murakami, S.; Noguchi, T.; Kinoshita, H.; Sekine, Y.; Iemura, S.; Natsume, T.; Ichijo, H. Mitochondrial phosphoglycerate mutase 5 uses alternate catalytic activity as a protein serine/threonine phosphatase to activate ASK1. *Proc. Natl. Acad. Sci. U.S.A.* **2009**, *106*, 12301–12305.

[42] Panda, S.; Srivastava, S.; Li, Z.; Vaeth, M.; Fuhs, S. R.; Hunter, T.; Skolnik, E. Y. Identification of PGAM5 as a mammalian protein histidine phosphatase that plays a central role to negatively regulate $CD4^+$ T cells. *Mol. Cell* **2016**, *63*, 457–469.

[43] Kim, Y.; Huang, J.; Cohen, P.; Matthews, H. R. Protein phosphatases 1, 2A, and 2C are protein histidine phosphatases. *J. Biol. Chem.* **1993**, *268*, 18513–18518.

[44] Duclos, B.; Marcandier, S.; Cozzone, A. J. Chemical properties and separation of phosphoamino acids by thin-layer chromatography and/or electrophoresis. *Methods Enzymol.* **1991**, *201*, 10-21.

[45] Li, H.-C.; Hsiao, K.-J.; Sampathkumar, S. Characterization of a novel alkaline phosphatase with a phosphorylase activity which phosphatase of communication. *J. Biol. Chem.* **1979**, *254*, 3368–3374.

[46] Leis, J. F.; Kaplan, N. O. An acid phosphatase in the plasma membranes of human astrocytoma showing marked specificity toward phosphotyrosine protein. *Proc. Natl. Acad. Sci. U.S.A.* **1982**, *79*(21), 6507–6511.

[47] Zhang, Z. Y.; Maclean, D.; Thieme-Sefler, A. M.; Roeske, R. W.; Dixon, J. E. A continuous spectrophotometric and fluorimetric assay for protein tyrosine phosphatase using phosphotyrosine-containing peptides. *Anal. Biochem.* **1993**, *211*, 7–15.

[48] Martin, D. R.; Dutta, P.; Mahajan, S.; Varma, S.; Stevens, S. M. Structural and activity characterization of human PHPT1 after oxidative modification. *Sci. Rep.* **2016**, *6*, 23658.

[49] McCullough, B. S.; Barrios, A. M. Facile, fluorogenic assay for protein histidine phosphatase activity. *Biochemistry* **2018**, *57*, 2584–2589.

[50] Itaya, K.; Ui, M. A new micromethod for the colorimetric determination of inorganic phosphate. *Clin. Chim. Acta* **1966**, *14*, 361–366.

[51] Attwood, P. V.; Ludwig, K.; Bergander, K.; Besant, P. G.; Adina-Zada, A.; Krieglstein, J.; Klumpp, S. Chemical phosphorylation of histidine-containing peptides based on the sequence of histone H4 and their dephosphorylation by protein histidine phosphatase. *Biochim. Biophys. Acta* **2010**, *1804*, 199–205.

[52] Kee, J. M.; Villani, B.; Carpenter, L. R.; Muir, T. W. Development of stable phosphohistidine analogues. *J. Am. Chem. Soc.* **2010**, *132*, 14327–14329.

[53] Kee, J.-M.; Oslund, R. C.; Perlman, D. H.; Muir, T. W. A pan-specific antibody for direct detection of protein histidine phosphorylation. *Nat. Chem. Biol.* **2013**, *9*, 416–421.

[54] Kee, J. M.; Oslund, R. C.; Couvillon, A. D.; Muir, T. W. A second-generation phosphohistidine analog for production of phosphohistidine antibodies. *Org. Lett.* **2015**, *17*, 187–189.

[55] Lilley, M.; Mambwe, B.; Thompson, M. J.; Jackson, R. F. W.; Muimo, R. 4-Phosphopyrazol-2-yl alanine: a non-hydrolysable analogue of phosphohistidine. *Chem. Commun.* **2015**, *51*, 7305–7308.

[56] Fuhs, S. R.; Meisenhelder, J.; Aslanian, A.; Ma, L.; Zagorska, A.; Stankova, M.; Binnie, A.; Al-Obeidi, F.; Mauger, J.; Lemke, G.; Yates III, J. R.; Hunter, T. (2015). Monoclonal 1- and 3-phosphohistidine antibodies: new tools to study histidine phosphorylation. *Cell* **2015**, *162*, 198–210.

[57] Smith, D. L.; Bruegger, B. B.; Halpern, R. M.; Smith, R. A. New histone kinases in nuclei of rat tissues. *Nature* **1973**, *246*, 103–104.

[58] Fraczyk, T.; Ruman, T.; Rut, D.; Dabrowska-Mas, E.; Ciesla, J.; Zielinski, Z.; Sieczka, K.; Debski, J.; Golos, B.; Winska, P.; Walajtys- Rode, E.; Shugar, D.; Rode, W. Histidine phosphorylation, or tyrosine nitration, affect thymidylate synthase properties. *Pteridines* **2009**, *20*, 137–142.

[59] Muimo, R.; Hornickova, Z.; Riemen, C. E.; Gerke, V.; Matthews, H.; Mehta, A. Histidine phosphorylation of annexin I in airway epithelia *J. Biol. Chem.* **2000**, *275*, 36632-36636.

[60] Hiromura, M.; Yano, M.; Mori, H.; Inoue, M.; Kido, H. Intrinsic ADP-ATP exchange activity is a novel function of the molecular chaperone, Hsp70. *J. Biol. Chem.* **1998**, *273*, 5435–5438.

[61] Ostrowski, W. Isolation of τ-phosphohistidine from a phosphoryl-enzyme intermediate of human prostatic acid phosphatase. *Biochim. Biophys Acta* **1978**, *526*, 147-153.

[62] Rose, Z. B. Evidence for a phosphohistidine protein intermediate in the phosphoglycerate mutase reaction. *Arch. Biochem. Biophys.* **1970**, *140*, 508−513.

[63] Gottlin, E. B.; Rudolph, A. E.; Zhao, Y.; Matthews, H. R.; Dixon, J. E. Catalytic mechanism of the phospholipase D superfamily proceeds via a covalent phosphohistidine intermediate. *Proc. Natl. Acad. Sci. U.S.A.* **1998**, *95*, 9202−9207.

[64] Attwood, P. V. P-N bond protein phosphatases. *Biochim. Biophys. Acta* **2013**, *1834*, 470–478.

# Chapter II. Development of Fluorescent Probes for Protein Histidine Phosphatases

This project was carried out in collaboration with Hoyoung Jung in our laboratory, and some of the experimental data also appear in her master's thesis.

## 2.1. Introduction – Fluorescent probes protein histidine phosphatases

Development of several research tools for studying protein histidine phosphorylation has facilitated better understanding of its biochemical and biological functions (refer to section 1.3). Nevertheless, more accurate and convenient tool for kinetic studies of protein histidine kinases/phosphatases are still desired because current tools are laborious or nonselective.

To address this, we aimed at the development of fluorescent-based activity probes for pHis phosphatases. Such chemical probes will enable convenient activity measurement of pHis phosphatases in continuous ways, greatly facilitating the kinetic studies of the enzymes. In addition, since these probes are based on real pHis functionality, they will provide more accurate kinetic data for these enzymes and they can potentially be specific to pHis phosphatases. In this chapter, two of our strategies are described: CHEF-based probes (refer to section 2.2) and naphthalimide-based probes (refer to section 2.3).

## 2.2. CHEF-based fluorescent probes for protein histidine phosphatases

### *2.2.1. Design and strategy*

In 2003, fluorescence probes based on the chelation-enhanced fluorescence (CHEF) effect was reported for protein kinase activities by the Imperiali group.[1] In CHEF effect, the fluorescence of a fluorophore is modulated upon the chelation to a metal cation. In that study, sulfonamido-oxine (Sox) was adapted as a CHEF-sensitive fluorophore, which was originally developed for zinc sensors.[2] When incorporated in a peptide substrate, Sox is little fluorescent without phosphorylation but it exhibits strong fluorescence upon phosphorylation of an adjacent amino acid residue due to the intramolecular chelation of $Mg^{2+}$ cation between Sox and the nascent phosphoryl group.[3] It was originally utilized for protein Ser/Thr/Tyr kinases, and further applied to pSer phosphatase activity of PP2A[4] and pTyr phosphatase activity of protein tyrosine phosphatase 1B (PTP1B).[5]

Our probe consists of two parts: Sox and a pHis-peptide substrate. We adopted the sequence around His18 of histone H4, a known peptide substrate for PHPT1. A series of histone H4 peptides were prepared by Fmoc-based solid-phase peptide synthesis (SPPS) with a cysteine mutation on the different positions.[6] The cysteine residue in each peptide, protected by 4-monomethoxytrityl (Mmt) group, was selectively deprotected in mild acidic condition and subsequently alkylated on resin with Sox bromide (Sox-Br). After the final cleavage, Sox-incorporated histone H4 peptides (Sox-H4) were obtained, and each of them was phosphorylated on its histidine residue with potassium phosphoramidate (PPA) to yield a series of phosphorylated Sox-H4 (Sox-H4P) probes. We prepared this series with varied position of Sox because the intramolecular $Mg^{2+}$ chelation and the CHEF effect should be dependent on the relative geometry between the Sox fluorophore and pHis.

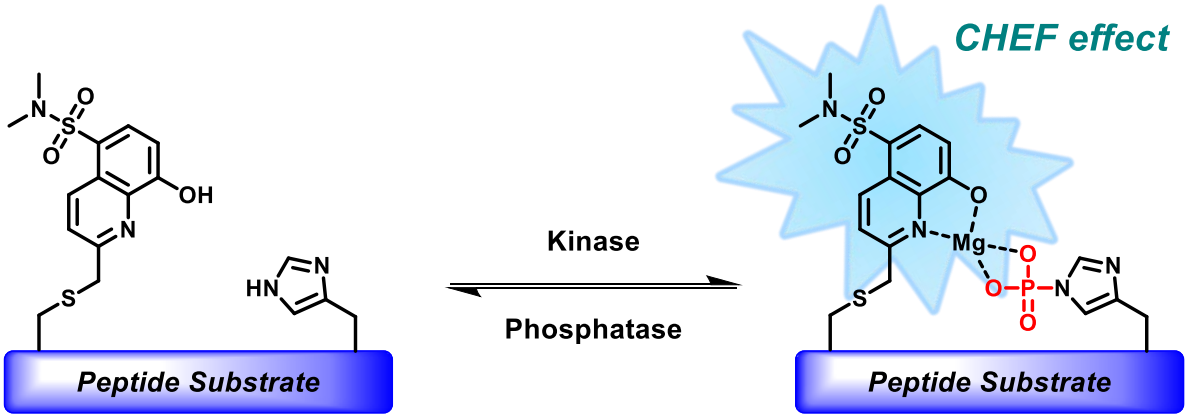


**Figure 8. Design of CHEF-based fluorescent probes.**

### *2.2.2. Synthesis*

#### *2.2.2.1. Synthesis of Sox-Br*

Sox-Br was prepared *via* 6 steps from 8-hydroxy-2-methylquinoline, following the published protocols with some improvements (Scheme 1). Especially in the last bromination step, the amount of N-bromosuccinimide (NBS) and triphenylphosphine were increased to 2.5 molar equivalent to compound **5** to fasten the reaction. As a result, the reaction was almost 10 times faster than the reported time, with comparable yield. The final product Sox-Br was completely dried and stored under -80°C. It has been stable for several months with negligible hydrolysis (typically less than 5%) to compound **5**.

#### *2.2.2.2. Synthesis of Cys-mutated histone H4 peptide via Fmoc-SPPS*

From the position of His, each amino acid residue on (-2) to (+3) position was changed into Mmt

protected Cys. Each of Cys-mutated histone H4 peptide was synthesized *via* Fmoc-SPPS on Rink amide resin. Protecting groups and the resin should not be cleaved because further alkylation with Sox-Br should be on the resin state.

**Scheme 1. Synthesis of Sox-Br.**

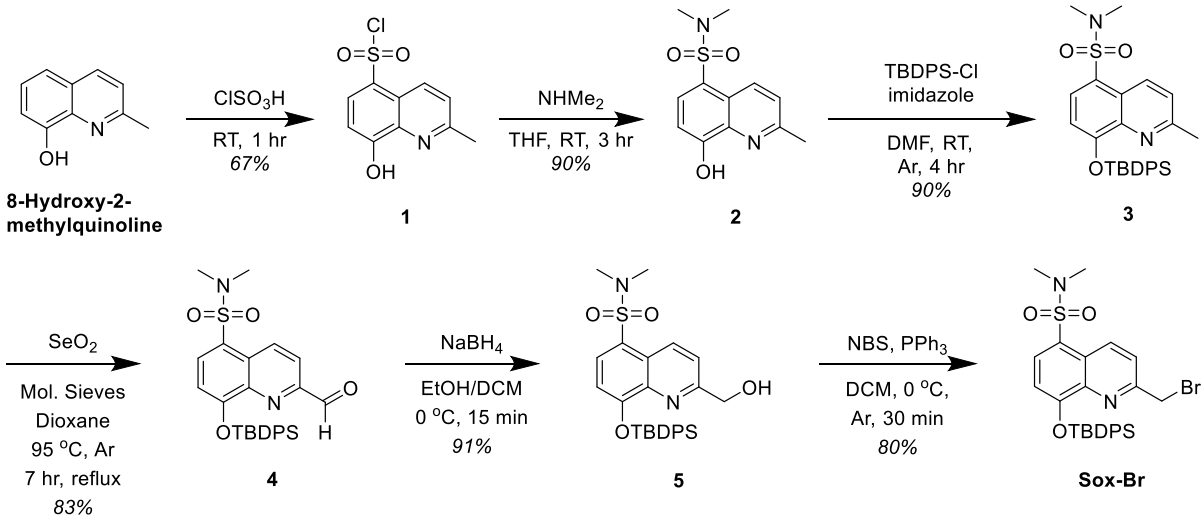


* TBDPS-Cl: tert-Butyldiphenylsilylchloride, NBS: N-Bromosuccinimide

#### *2.2.2.3. Selective Mmt deprotection and on-resin alkylation*

Mmt is a hyper acid-labile protecting group, so it can be easily deprotected under 1% TFA. Under this condition, other acid-labile protecting groups such as trityl (Trt) and tert-Butyloxycarbonyl (Boc) group are hardly deprotected. Therefore, only the thiol of Cys can be unmasked while other side chains are still protected.

Then, 2 molar equivalence of Sox-Br was added to form Cys-Sox (C-Sox) by nucleophilic attack. According to the published protocols, 1,1,3,3-tetramethylguanidine (TMG) was used as a non-nucleophilic base, but we observed that Sox-Br was degraded into unidentified products in the presence of TMG. Accordingly, TMG was replaced to *N,N*-diisopropylethylamine (DIPEA), a milder non-nucleophilic base. After the reaction, the peptide cleavage from the resin as well as the removal of all the remaining protecting groups were carried out under 95% TFA. The crude product was analyzed and purified *via* high performance liquid chromatography (HPLC) to provide Sox-H4 (52% yield).

#### *2.2.2.4. Selective chemical phosphorylation of histidine residue with PPA*

The histidine residue of each Sox-H4 series was phosphorylated with excess amount of PPA in pH

8 buffer. PPA is known phosphorylating reagent which can selectively phosphorylate histidine.[7] According to the HPLC analysis of the reaction mixture, up to 90% of Sox-H4 was phosphorylated. To remove remaining Sox-H4 and excess phosphates, it was purified *via* semi-preparative HPLC to yield the series of Sox-H4P. Purified samples were basified to pH 9 using ammonium hydroxide and they were stored under -80°C for later use without meaningful hydrolysis to Sox-H4.

The Sox incorporation and histidine phosphorylation in our series of Sox-H4P were validated *via* liquid chromatography-tandem mass spectrometry (LC-MS/MS) in collaboration with Prof. Jeong Kon Seo at UNIST Central Research Facilities. We used both collision-induced dissociation (CID) and electron-transfer dissociation (ETD) methods for the MS/MS analysis, and the latter provided clearer and more precise data for our probes (refer to section 2.5).

**Scheme 2. Synthesis of CHEF-based fluorescent probe, Sox-H4P.**

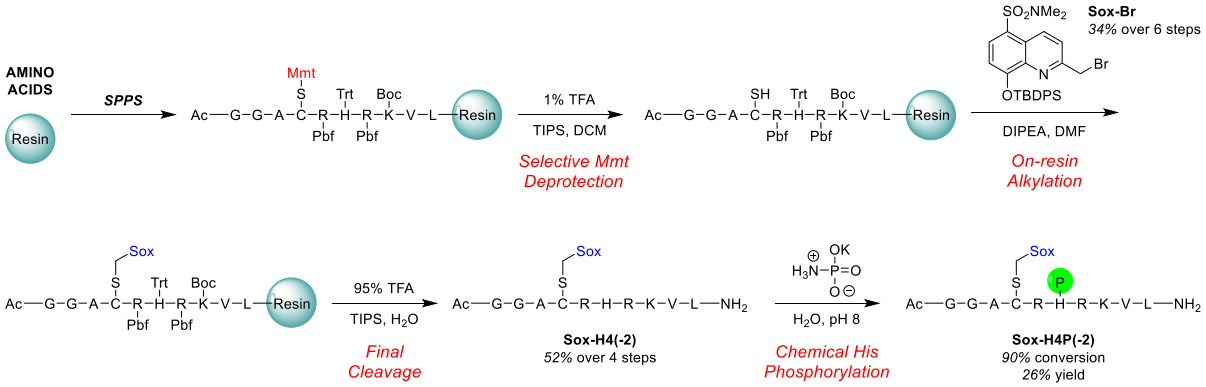


### *2.2.3. Validation and optimization*

Next, the position of C-Sox was optimized to maximize the CHEF effect of Sox-H4P (Table 2). Since the CHEF effect is dependent on the molecular geometry between the C-Sox and the phosphoryl group, it is necessary to prepare and test a series of probes with C-Sox at different positions around the pHis. The fluorescent increase between each Sox-H4 and the corresponding Sox-H4P was compared (Table 2). Among them, Sox-H4P(-2), the probe with C-Sox located at the (-2) position of pHis, showed the largest fluorescence increase (3.0 ± 0.1 fold). Indeed, in the case of already reported Sox-based probes, (-2) or (+2) position of C-Sox was recommended by the Imperiali group because the chelation of $Mg^{2+}$ between C-Sox and phosphorylation site is generally optimal in that distance.

Next, we determined the dissociation constant ($K_d$) of Sox-H4(-2) and Sox-H4P(-2) to $Mg^{2+}$ (Figure 9A). As expected, Sox-H4P(-2) showed lower $K_d$ value (102 ± 9 mM) than Sox-H4(-2) (177 ± 30 mM). It means that our probe has higher affinity to $Mg^{2+}$ upon phosphorylation. For this probe, the

fluorescence increase determined at various $Mg^{2+}$ concentrations. Sox-H4P(-2) showed maximum fluorescence increase at 20 mM of $MgCl_2$, so this concentration was used for further assays (Figure 9B).

**Table 2. Optical properties of Sox-H4P series with different C-Sox positions.**

| Entry | Peptide substrate sequence | | | | | | | | | | | | Fold fluorescence increase |
|---|---|---|---|---|---|---|---|---|---|---|---|---|---|
| | N | -5 | -4 | -3 | -2 | -1 | **0** | +1 | +2 | +3 | +4 | C | |
| **Sox-H4(-2)** | Ac | G | G | A | C-Sox | R | **H** | R | K | V | L | $NH_2$ | 3.0 ± 0.1 |
| **Sox-H4(-1)** | Ac | G | G | A | K | C-Sox | **H** | R | K | V | L | $NH_2$ | 1.6 ± 0.1 |
| **Sox-H4(+1)** | Ac | G | G | A | K | R | **H** | C-Sox | K | V | L | $NH_2$ | 1.5 ± 0.1 |
| **Sox-H4(+2)** | Ac | G | G | A | K | R | **H** | R | C-Sox | V | L | $NH_2$ | 2.6 ± 0.2 |
| **Sox-H4(+3)** | Ac | G | G | A | K | R | **H** | R | K | C-Sox | L | $NH_2$ | 2.0 ± 0.1 |

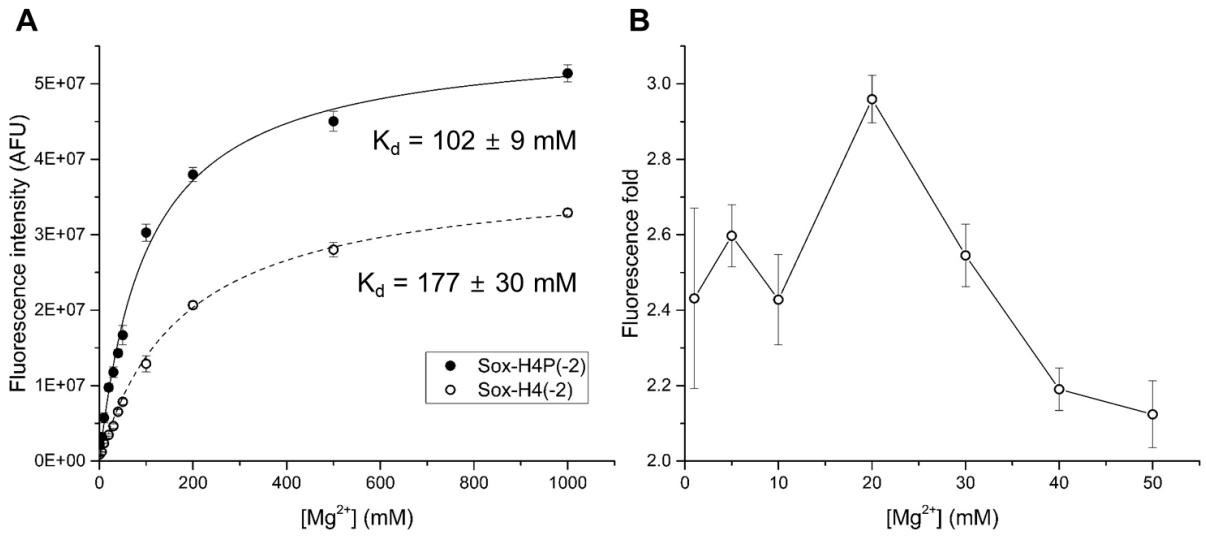


**Figure 9. (A) Measurement of $Mg^{2+}$ $K_d$ for Sox-H4(-2) and Sox-H4P(-2). (B) Fluorescence fold between Sox-H4(-2) and Sox-H4P(-2) upon the concentrations of $Mg^{2+}$.**

We also checked the relationship between the fluorescence intensity and the degree of phosphorylation to determine whether it can be easily quantified by simple fluorescence measurement. To our delight, it showed excellent linear relationship (Figure 10A). The fluorescence intensity was also almost perfectly proportional to the probe concentration, which was independently quantified by NMR and HPLC peak areas (Figure 10B). Thus, phosphorylation and dephosphorylation of our probe can be directly quantified by simple fluorescence measurement.

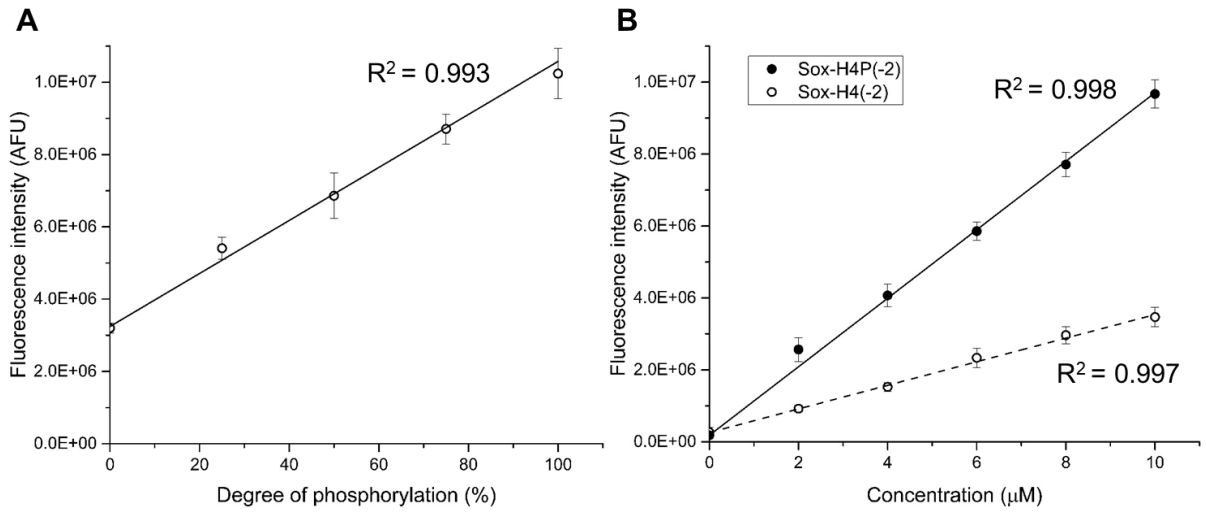


**Figure 10. (A) Linearity of the fluorescence increase upon phosphorylation of Sox-H4(-2). (B) Linearity of the fluorescence increase upon concentrations of Sox-H4(-2) and Sox-H4P(-2).**

### *2.2.4. In vitro phosphatase activity assays*

With the optimized Sox-H4P, we first performed the enzymatic activity assays with PHPT1. To our delight, the fluorescence intensity of Sox-H4P decreased over time upon incubation with PHPT1 (Figure 11). Complete dephosphorylation of Sox-H4P in this reaction mixture was independently confirmed by HPLC. We also used PHPT1 H53A mutant, whose phosphatase activity is totally lost, and our probe showed little fluorescence change when treated with this mutant. These results show that our probe is indeed enzymatically dephosphorylated by PHPT1. Accordingly, Sox-H4P can be used for real-time monitoring of pHis phosphatase activity.

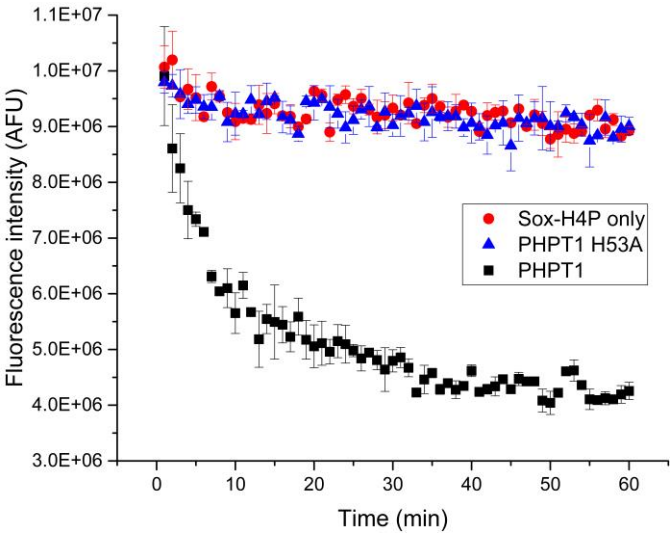


**Figure 11. Real-time measurement of dephosphorylation of Sox-H4P by PHPT1.**

To demonstrate that we can conveniently determine the kinetic parameters of PHPT1 using our probe, we performed PHPT1-mediated pHis dephosphorylation assay using various concentrations of Sox-H4P (Figure 12A). Each dephosphorylation graph was fitted to the pseudo-first order equation to calculate the initial reaction rate, and then it was plotted *versus* the concentration of the Sox-H4P substrate. This graph was fitted to Michaelis-Menten equation to obtain the kinetic parameters of PHPT1 (Figure 12B).

Previously reported kinetic parameters were determined using non-specific small molecule substrates pNPP ($K_M$ = 8.81 mM, $k_{cat}$ = 0.10 $sec^{-1}$, $k_{cat}/K_M$ = 11.35 $M^{-1}sec^{-1}$) and DiFMUP ($K_M$ = 220 μM, $k_{cat}$ = 0.39 $sec^{-1}$, $k_{cat}/K_M$ = 1800 $M^{-1}sec^{-1}$), and these values are much smaller than our values ($K_M$ = 16.13 ± 3.94 μM, $k_{cat}$ = 3.06 ± 0.32 $sec^{-1}$, $k_{cat}/K_M$ = 1.90 × $10^5$ ± 5.04 × $10^4$ $M^{-1}sec^{-1}$) because they are not actual pHis substrate. From the same reason, they are less sensitive to PHPT1, so much larger amount of enzyme and substrate are needed. On the other hand, Sox-H4P is much closer to phosphorylated histone H4, the real substrate for PHPT1. Therefore, far more reliable kinetic parameters can be obtained with less consumption of materials.

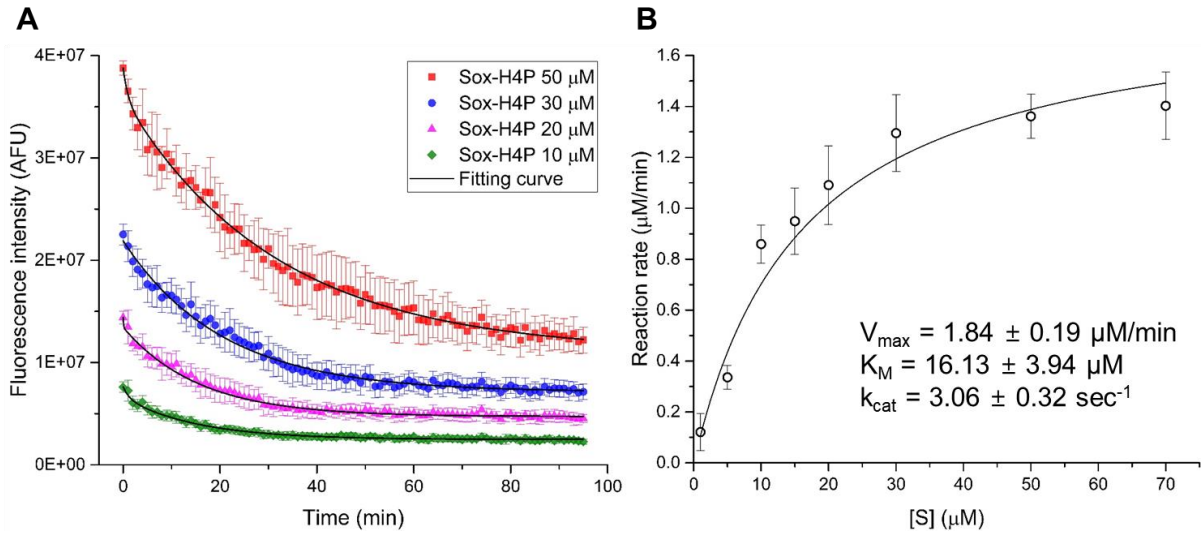


**Figure 12. (A) Fluorescence assay of PHPT1 activity with various concentrations of Sox-H4P. (B) Michaelis-Menten saturation curve for PHPT1-catalyzed dephosphorylation of Sox-H4P.**

Next, we investigated the specificity of Sox-H4P using various phosphatases. If our probe is selective to specific phosphatases, it will be very useful to monitor their enzyme activity. We tested LHPP and PP2C, previously reported to possess pHis phosphatase activities, and other phosphatases including alkaline phosphatase ALPP, pTyr phosphatase PTP1B, and pArg phosphatase YwlE.

Interestingly, Sox-H4P was dephosphorylated by PHPT1 only. Any other phosphatase (LHPP, ALPP, PTP1B, and YwlE) was inactive towards our probe. This result shows the potential value of Sox-H4P as the PHPT1-selective probe.

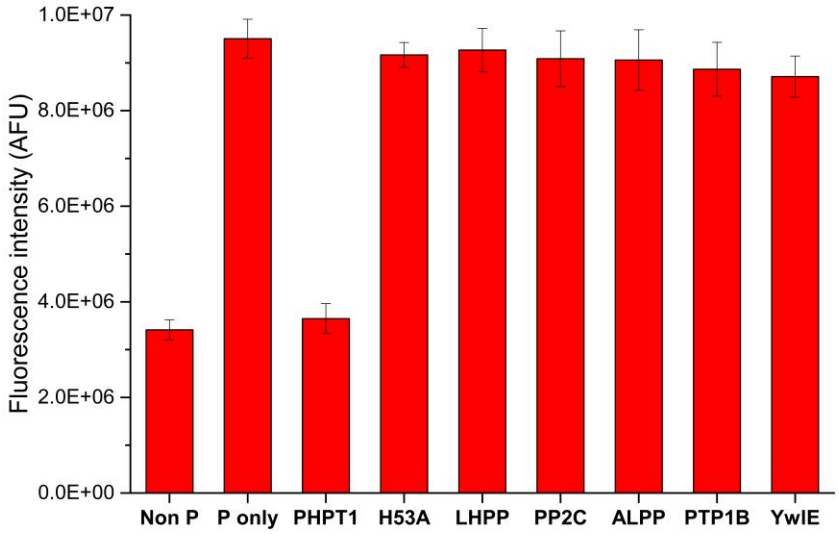


**Figure 13. Relative dephosphorylation activity of various phosphatases to Sox-H4P.**

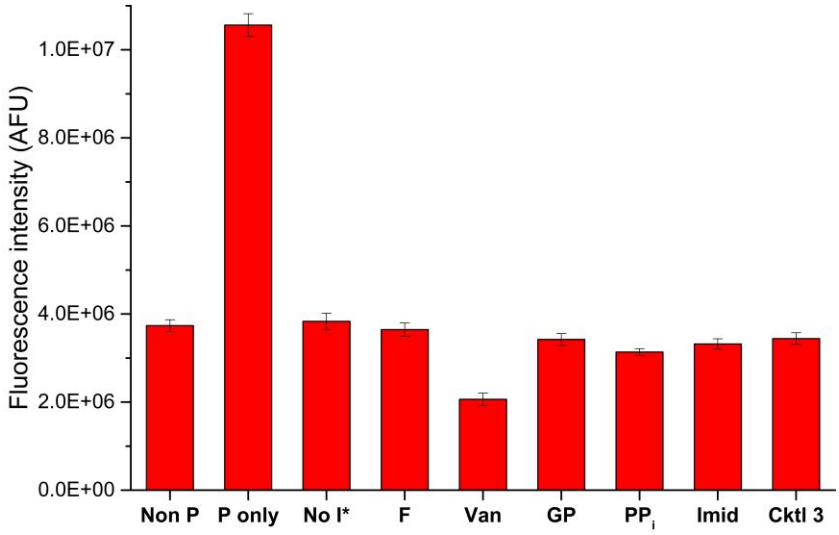


**Figure 14. Activity test of common phosphatase inhibitors to PHPT1. I*: inhibitors, F: fluoride, Van: vanadate, GP: glycerophosphate, $PP_i$: pyrophosphate, Imid: imidazole, Cktl 3: Phosphatase Inhibitor Cocktail III.**

PHPT1 has been implicated in several cancers, hence its inhibitor can be a potential drug target for cancer metastasis. However, no inhibitor is known for PHPT1 yet, so we tested a number of potential

PHPT1 inhibitors using our probe. We used several common phosphatase inhibitors such as sodium fluoride, sodium orthovanadate, sodium glycerophosphate, sodium pyrophosphate, imidazole, and Phosphatase Inhibitor Cocktail III (a mixture of cantharidin, (-)-*p*-bromolevamisole oxalate, and calyculin A) from Sigma Aldrich. As the result, there was no inhibition of PHPT1 by any general inhibitor. In case of vanadate, glycerophosphate, and pyrophosphate, additional $MgCl_2$ was added to the reaction mixture to compensate the presumed competing chelation to $Mg^{2+}$. Especially, fluorescence decrease by vanadate was too large to be recovered to the original value.

Lastly, we tried to monitor the dephosphorylation of Sox-H4P in cell lysate. Since our probe was specific to PHPT1 and no common inhibitor could inhibit PHPT1, with common inhibitors, we could observe the activity of PHPT1 only. We prepared HeLa cell lysate and inhibitor mixtures which consisted of fluoride, imidazole, and Phosphatase Inhibitor Cocktail III.

To our delight, fluorescence decrease of our probe was observed in HeLa cell lysate with or without inhibitor mixture (Figure 15). Furthermore, kinetics in both of them were similar, suggesting dephosphorylation of Sox-H4P was likely catalyzed by PHPT1 only. In the presence of excess amount of exogenously added PHPT1, Sox-H4P was almost immediately dephosphorylated. From these results, pHis phosphatase activity of PHPT1 in HeLa cell lysate was indirectly confirmed. Inspired by this data, we will test the pHis phosphatase activity of PHPT1-knockdown cell lysates with our probe.

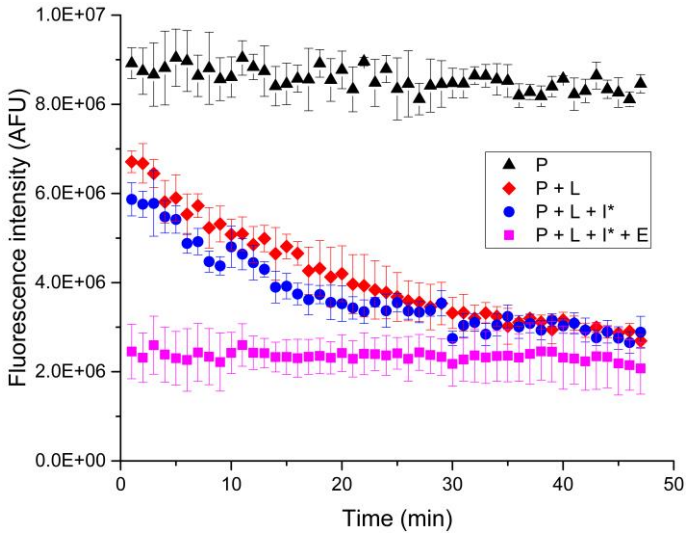


**Figure 15. Dephosphorylation of Sox-H4P in phosphatases-inhibited HeLa cell lysate. P: probe, L: lysate, $I^*$: inhibitors, E: enzyme.**

## 2.3. Naphthalimide-based fluorescent probes for protein histidine phosphatases

### *2.3.1. Design and strategy*

While our CHEF-based fluorescent probe Sox-H4P has demonstrated the feasibility of real-time measurement of PHPT1 activities, it has limitation of fluorescence turn-off upon dephosphorylation by the phosphatase. To address this limitation, we set out to develop a fluorescence turn-on probe for PHPT1, which should be easier to monitor.

Recently, naphthalimide-based probes were reported, of which fluorescence was quenched when the imidazole moiety was *N*-glycosylated[8] or coordinated to $Hg^{2+}$.[9] Their fluorescence was also restored by unmasking the nitrogen atom. It was ascribed to the intramolecular H-bonding between the carbonyl group of naphthalimide and the imidazole. In addition, naphthalimide-pHis intermediate was postulated in the histidine-catalyzed hydrolysis of ATP.[10] Inspired by these, we hypothesized that phosphorylation of the imidazole could quench the fluorescence in a similar way.

We designed three sets of naphthalimide-based fluorescent probes: HN (histidine + naphthalimide), HMeN (histidine methyl ester + naphthalimide), and HMeBN (histidine methyl ester + bromo-naphthalimide). All of them are phosphorylated to yield HN-P, HMeN-P, and HMeBN-P, respectively.

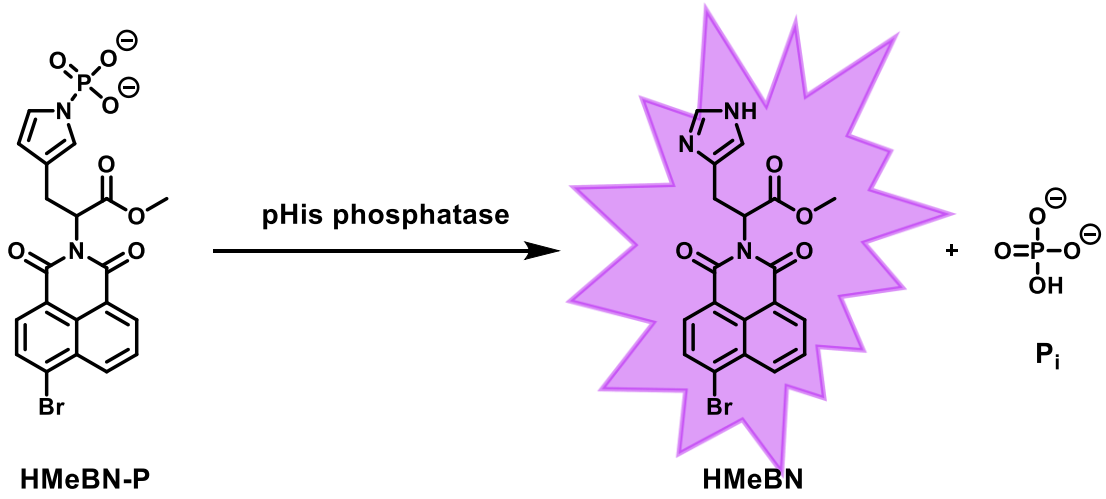


**Figure 16. Initial design of naphthalimide-based fluorescent probe.**

### *2.3.2. Synthesis*

Compared to CHEF-based fluorescent probes, naphthalimide-based fluorescent probes can be synthesized much more easily in two steps. 4-Bromo-1,8-naphthalic anhydride and L-histidine methyl ester react to yield HMeBN. Likewise, 1,8-naphthalic anhydride reacts with L-histidine methyl ester and L-histidine to yield HMeN and HN, respectively. After the purification, all of them are subsequently

phosphorylated. HMeBN and HMeN are phosphorylated by phosphoryl chloride ($POCl_3$) and following hydrolysis to form HMeBN-P and HMeN-P, respectively. HN can be phosphorylated by PPA in pH 8 water to form HN-P.

**Scheme 3. Synthesis of naphthalimide-based fluorescent probes.**

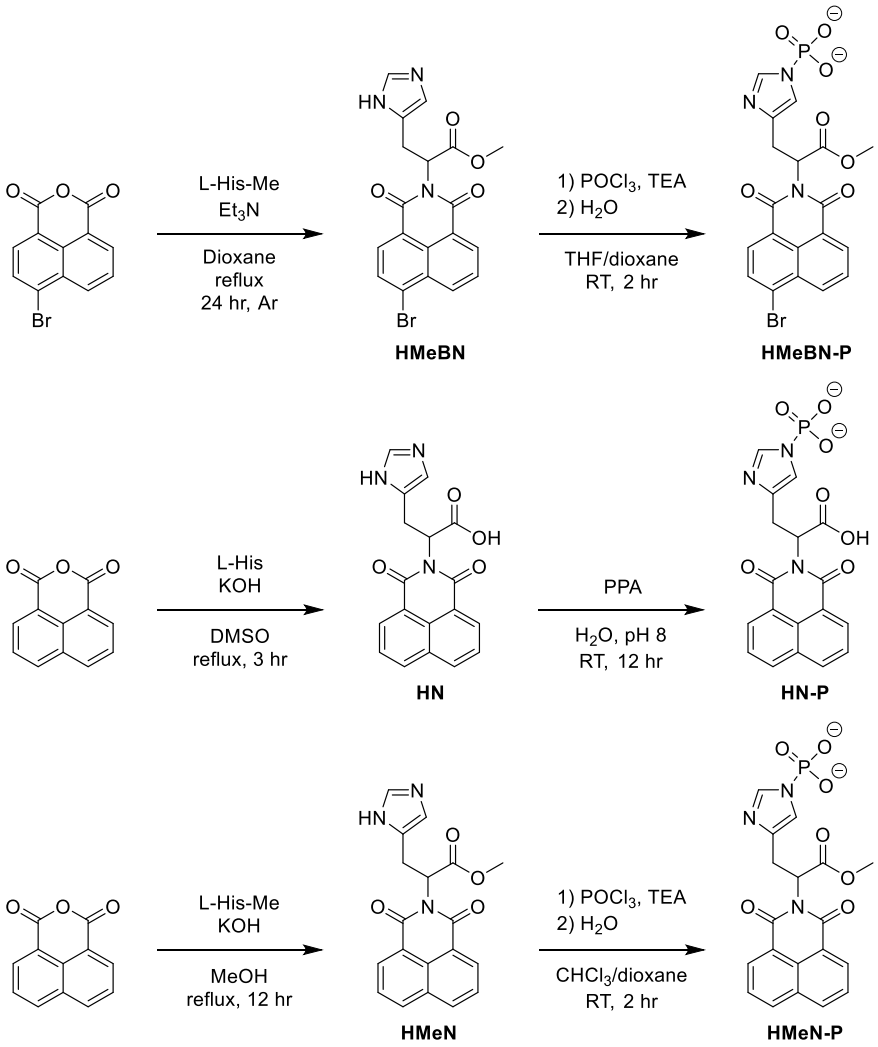


### *2.3.3. Validation and optimization*

To choose the best candidate, we compared three naphthalimide-based probes: HN-P, HMeN-P, and HMeBN-P. In terms of convenience, HMeBN-P is the easiest to be phosphorylated with $POCl_3$ because HMeBN is well soluble in THF while HN and HMeN are not. HN was the only water-soluble derivative without phosphorylation, so it can be phosphorylated with PPA in aqueous buffers, but it needs excess amount of PPA for complete phosphorylation. Another advantage of HMeBN-P is that it

can be easily isolated from HMeBN by extraction with chloroform. HMeBN-P is well soluble in water but not in chloroform, and HMeBN is has the opposite solubility pattern. HN-P and HN are both soluble in water, so they are hardly separable without using HPLC. In addition, HMeN-P and HMeBN-P have larger fluorescence fold decrease upon their dephosphorylation by PHPT1 (refer to section 2.3.4). To sum up, we selected HMeBN-P as an optimal naphthalimide-based fluorescent probe for further assays.

Before the pHis phosphatase assays, we tried to study the fluorescent mechanism of naphthalimide probes. According to the literature,[8,9] it is assumed to be strongly related to p$K_a$ of the imidazole moiety. We took $^1$H-NMR and the fluorescence of HMeBN at various pH. At low pH, imidazole *N*-protonation occurs, thereby deshielding protons at C2 and C4 (Figure 17). We also plotted fluorescence intensities of HMeBN and HMeBN-P. Upon phosphorylation, positive charge of imidazole ring is delocalized through resonance stabilization.[11] Both graphs were perfectly fitted to the sigmoidal function ($R^2$ > 0.99). Center points of sigmoidal graph are 7.03 for C2 and 7.05 for C4, almost corresponding to p$K_a$ of imidazole ring. This result suggests that the mechanism of histidine naphthalimide probes is concerned with imidazole *N*-protonation of histidine residue. Further studies are in progress to elucidate the fluorescence turn off mechanism.

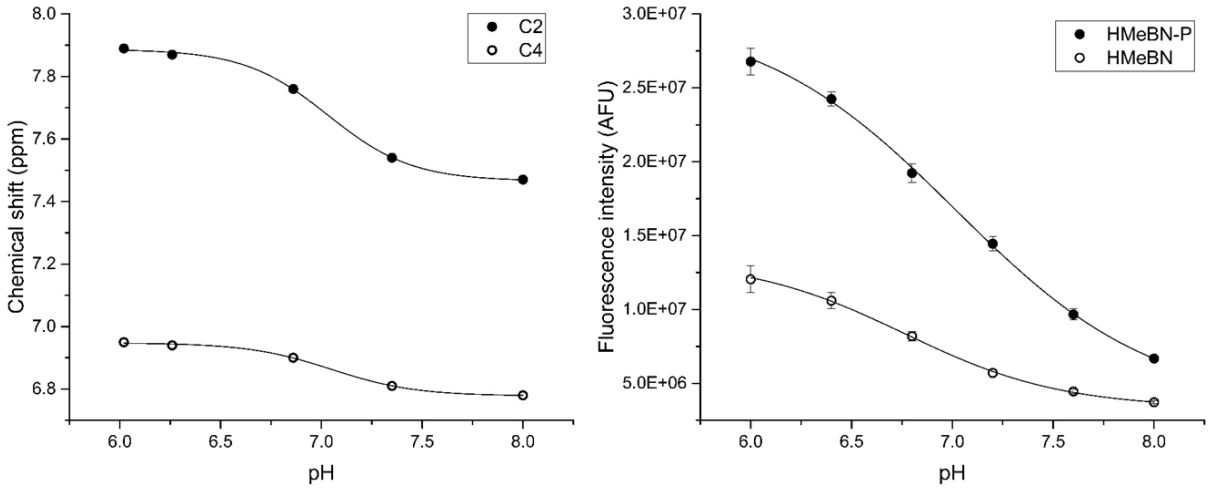


**Figure 17. Sigmoidal pH-dependency of HMeBN(-P).**

### *2.3.4. In vitro phosphatase activity assays*

Before the further assays, we had to compare three probes in terms of their fluorescence change upon dephosphorylation ($\lambda_{ex}$ = 340 nm, $\lambda_{em}$ = 390 nm for HN-P, $\lambda_{ex}$ = 350 nm, $\lambda_{em}$ = 400 nm for HMeN-P, and $\lambda_{ex}$ = 360 nm, $\lambda_{em}$ = 410 nm for HMeBN-P). Contrary to our expectation, all of three probes showed fluorescence decrease upon dephosphorylation by PHPT1. They did not correspond to the design as fluorescence turn-on probes, but we decided to take them as fluorescence turn-off probes for

protein histidine phosphatases. While this is not as ideal as our original design, we regarded this as a potentially superior alternative to our Sox-based peptide probes since the synthesis is more convenient.

Under the same reaction condition, probes with methyl ester (HMeN-P and HMeBN-P) showed larger fluorescence decrease than the probe without methyl ester (HN-P). Of the two, HMeBN-P had convenience in synthesis, so we adapted it as the optimal naphthalimide-based probe.

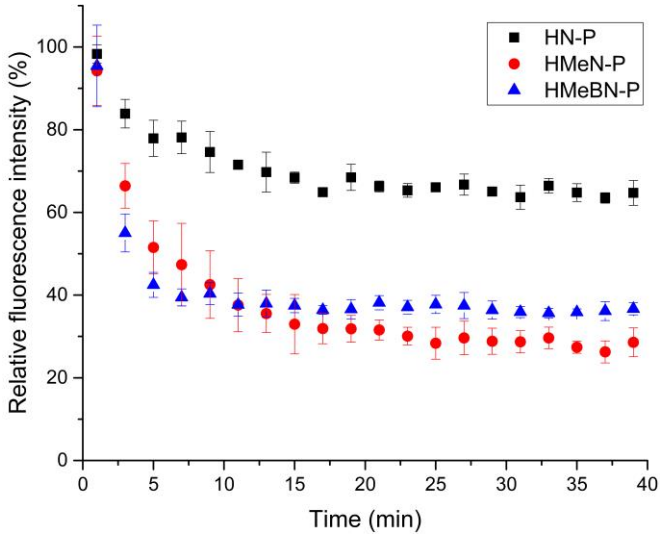


**Figure 18. PHPT1-mediated dephosphorylation of naphthalimide-based probes.**

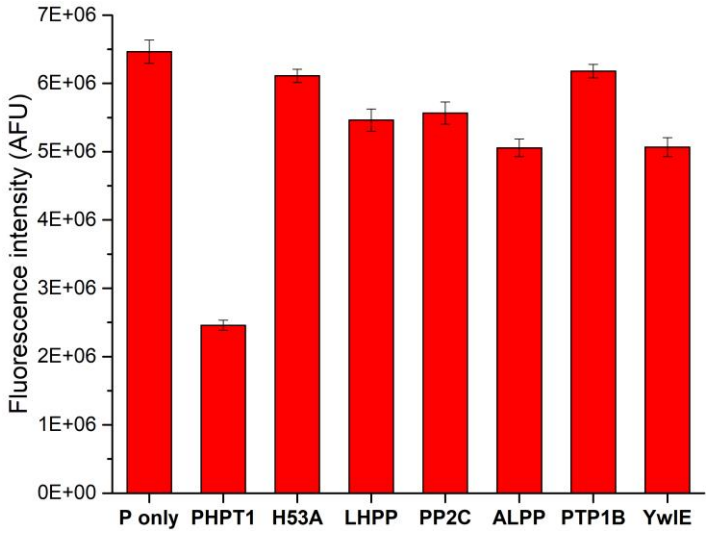


**Figure 19. Relative dephosphorylation activity of various phosphatases to HMeBN-P.**

Same as the case of CHEF-based fluorescent probe Sox-H4P, we investigated the specificity of HMeBN-P using various phosphatases. Unlike Sox-H4P, we did not expect high specificity because it

is a small molecule probe, not pHis peptide substrate. Surprisingly, we obtained similar result that HMeBN-P was specific to PHPT1 like Sox-H4P. Especially, we expected that LHPP could dephosphorylate HMeBN-P because we already checked free pHis as a target of LHPP by simple TLC experiment (data not shown). However, other phosphatases including LHPP, PP2C, ALPP, PTP1B, and YwlE showed a little or no phosphatase activities towards our probe. All the reaction mixtures were also analyzed *via* HPLC to confirm the probes were indeed dephosphorylated. This result shows the potential application of HMeBN-P as a PHPT1-selective probe.

## 2.4. Conclusion and future direction

Though the biological significance of PHPT1 has been increasingly recognized over recent years, there was still no suitable research tools for continuous measurement of its kinetics. To overcome this, we developed two types of fluorescent probes for protein histidine phosphatases. One is a CHEF-based probe Sox-H4P which showed weaker fluorescence upon dephosphorylation, and the other is a naphthalimide-based small-molecule probe HMeBN-P. Both types our probes exhibited fluorescence turn-off upon dephosphorylation.

Our probes contain actual pHis in their structures, facilitating more accurate kinetic analysis of PHPT1. Indeed, we obtained Michaelis-Menten parameters which are different in orders of magnitude from previously reported values using pNPP or DiFMUP, demonstrating the limitation of detecting the enzyme kinetics using non-pHis substrates.

Both Sox-H4P and HMeBN-P have great selectivity to PHPT1. Using this feature, we performed *in vitro* PHPT1 inhibition assays and confirmed that there was no inhibitor for PHPT1. With our fluorescent probes, we can discover novel inhibitor for PHPT1 *via* high-throughput screening. Furthermore, we can detect the pHis phosphatase activity of PHPT1 in phosphatase-inhibited HeLa cell lysate. We believe these tools can significantly facilitate the biological studies and potential drug discovery efforts on PHPT1.

## 2.5. Experimental Data

### *2.5.1. General materials*

All reagents were purchased from Alfa Aesar (Ward Hill, MA) or Tokyo Chemical Industry Co., LTD. (Tokyo, Japan) without further purification unless otherwise noted. All biological reagents (unless otherwise noted) were purchased from Bio-rad (Hercules, CA). All buffering salts and organic solvents were purchased from Daejung (Siheung, Republic of Korea) and Samchun (Pyeongtaek, Republic of Korea). Tris/HCl salt and HisPur Ni-NTA Resin were purchased from Fisher Scientific (Pittsburgh, PA). Dithiothreitol (DTT) and Adenosine 5'-diphosphate sodium salt (ATP) were purchased from Sigma-Aldrich (St. Louis, MO). Coomassie brilliant blue, glycerol and magnesium chloride hexahydrate were purchased from Biosesang (Seongnam, Republic of Korea). HBTU and Rink-amide resin were purchased from Matrix innovation (Quebec, Canada). Fmoc-Cys(Mmt)-OH was purchased from Bepharm (Shanghai, China). All amino acids used in peptide synthesis (unless otherwise noted) were purchased from GL Biochem (Shanghai, China). LB Broth and LB Agar were purchased from Affymetrix (Santa Clara, CA). Ampicillin sodium salt and Isopropyl β-D-1-thiogalactopyranoside (IPTG) were purchased from MP Biomedicals (Santa Ana, CA). Protein phosphatase 2C isoform alpha (PP2C), placental alkaline phosphatase (ALPP), and protein tyrosine phosphatase 1B (PTP1B) were purchased from Sino Biological (Beijing, China). Sodium fluoride, sodium orthovanadate, and Phosphatase Inhibitor Cocktail III were purchased from Sigma-Aldrich.

### *2.5.2. General methods*

Analytical RP-HPLC was performed on Agilent 1200 series instruments equipped with a C18 InertSustain (5 μm, 4.6 x 150 mm, GL Sciences, Tokyo, Japan) column at a flow rate of 1 mL/min employing gradients of solvent A (0.1% TFA in water) and solvent B (90% acetonitrile in water with 0.1% TFA). For all analytical RP-HPLC runs a two-minute isocratic period in initial conditions was followed by 8 or 20-minute linear gradient with increasing solvent B concentration. The solvent gradients are specified in each of HPLC experiment (see below). We performed semi-preparative RP-HPLC with a C18 InertSustain (5 μm, 10 x 250 mm) at a flow rate of 2.5 mL/min. All semi-preparative RP-HPLC runs were carried out employing gradients of solvent A (0.1% TFA in water) and solvent B (90% acetonitrile in water with 0.1% TFA) with an initial five-minute isocratic period followed by a 20 or 40-minute linear gradient with increasing solvent B concentration. Cells were lysed using a VC-750 Watts Ultrasonic Processor (Sonics & Materials, Inc., Newtown, CT). Samples were lyophilized on a Scanvac CoolSafe Freeze Dryer (LaboGene, Allerød, Denmark). pH of buffer was measured with a pH meter, Orion Star A211 (Thermo Scientific, Waltham, MA). Mass were measured with Ultraflex III-MALDI-TOF/TOF (Bruker BioSpin, Billerica, MA) or Q Exactive Hybrid Quadrupole-Orbitrap mass

spectrometer (Thermo Scientific, Waltham, MA). Absorbance was measured with V-670 UV-VIS-NIR spectrophotometer (JASCO, Easton, MD). Fluorescence was measured with SpectraMax i3x microplate reader (Molecular Devices, Sunnyvale, CA).

### *2.5.3. General synthetic materials and methods*

All chemicals and solvents were obtained from Alfa Aesar or TCI unless otherwise noted and used without further purification unless otherwise noted. Silica gel (pore size 60 Å, mesh particle size 200-400) was purchased from Sigma-Aldrich. Florisil (mesh particle size 60-100) was purchased from J.T Baker (Center Valley, PA). Silica gel 60 aluminum-backed thin-layer chromatography (TLC) plates were purchased from EMD Chemicals (Billerica, MA). Chloroform-d, methanol-d4 and deuterium oxide NMR solvents were purchased from Cambridge Isotope Laboratories, Inc. (Andover, MA). Anhydrous solvents were obtained by incubation with activated molecular sieves following published protocols.[12] Unless otherwise noted, all reactions were carried out in an oven-dried (120°C) round-bottom flask equipped with a Teflon coated magnetic stir bar and a rubber septum under a positive pressure of argon atmosphere. Rotary evaporation was performed using a Rotavapor R-210 (Büchi, Flawil, Switzerland) equipped with a DryFast Diaphragm pump 2047 (Welch, Mt. Prospect, IL) and RW-0525G Low Temperature Bath Circulator (Jeiotech, Daejeon, Korea). Flash chromatography over silica gel was performed according to the method described by Still.[13] Compounds were visualized on TLC plates by irradiation with 254 nm UV light. Alternatively, the TLC plate was heated with Stanley Heat Gun STEL670 (Zhejiang Prulde Electric Appliance Co., Ltd., Zhejiang, China) following treatment with a solution of ninhydrin, *p*-anisaldehyde or potassium permanganate. Product yields refer to pure compounds, unless otherwise indicated.

### *2.5.4. NMR spectroscopy*

$^{1}$H NMR spectra were recorded on a Bruker 400 AVANCE III HD (Bruker BioSpin, Billerica, MA). $^{1}$H NMR chemical shifts are reported in parts per million (ppm) and are referenced relative to the residual solvent proton signal for $CDCl_3$ at 7.26 ppm, methanol-d4 at 3.31 ppm, and $D_2O$ at 4.79 ppm. $^{1}$H NMR data are tabulated in the following format: chemical shift, multiplicity [singlet (s), broad singlet (brs), doublet (d), triplet (t), multiplet (m)], coupling constant [Hz], number of protons. $^{13}$C NMR spectra were recorded on a Bruker 400 AVANCE III HD (Bruker BioSpin, Billerica, MA). $^{13}$C NMR chemical shifts are reported in ppm relative to carbon signals for $CDCl_3$ at 77.16 ppm, methanol-d4 at 49.00 ppm or, in $D_2O$, they are reported relative to the solvent deuterium signal.[14] $^{13}$C NMR data are tabulated in the following format: chemical shift, multiplicity [doublet (d)] (if applicable), coupling

constant [Hz]. $^{31}$P NMR spectra were recorded on a Bruker 400 AVANCE III HD (Bruker BioSpin, Billerica, MA). $^{31}$P NMR chemical shifts are reported relative to the solvent deuterium signal.[15]

### *2.5.5. General protocols of Fmoc-based solid phase peptide synthesis (Fmoc-SPPS)*

The peptides were synthesized on Rink amide resin (100-200 mesh, 1% DVB, 0.53 mmol/g) (Matrix innovation, Quebec, Canada) on a 0.1 mmol scale. The resin was swollen by incubating it in DMF with gentle agitation by $N_2$ bubbling. After 30 min, the resin was washed with 2 flow washes and one final batch wash with DMF. All the subsequent resin washing steps were carried out using this method. Fmoc deprotection was carried out using a 20% piperidine in DMF in two steps (1 min incubation and 20 min deprotection). Then, the resin was washed. Fmoc-amino acids were coupled using HBTU/ DIPEA as the activating agents. Desired amino acid (0.5 mmol) was weighted and dissolved in 0.49 M HBTU solution (in DMF) and immediately DIPEA (1 mmol) was added. The mixture was thoroughly mixed and allowed to be activated for 5 min, and the solution was poured into the resin. The reaction mixture was bubbled with $N_2$ for 30 minutes. Then, the resin was washed. With the last N-terminal residue, the acetylation was performed by incubating the resin with 20 mol equiv. of $Ac_2O$, 40 mol equiv. of DIPEA in DMF for 10 min (repeated 2 times). The peptide was cleaved from the resin by treatment with a mixture of 95% TFA, 2.5% TIPS, and 2.5% water for 1 hr at r.t. The crude peptide was precipitated in ice-cold ethyl ether, and was collected by filtration or centrifugation, and then dissolved in 50% HPLC solvent B to separate from the resin. The crude peptide was then purified by semi-preparative RP-HPLC.

### *2.5.6. General procedure for real-time phoshphatase activity assay*

Dephosphorylation assay with phosphatases was performed in 50 mM Tris, 150 mM NaCl, and 1 mM EDTA at pH 7.5 buffer. Unless noted otherwise, 10 μM of Sox-H4P, 20 mM of $MgCl_2$, and 10 nM of phosphatases were used. The enzyme activities were monitored by periodically measuring the fluorescence ($\lambda_{ex}/\lambda_{em}$ = 360/500 nm) at 25°C in a plate reader. Total reaction volume was 200 μL.

In the case of HMeBN-P, 10 μM of the probe and 100 nM of phosphatases were used without addition of $MgCl_2$, and 1% DMSO was added to the buffer. Fluorescence was measured at $\lambda_{ex}/\lambda_{em}$ = 360/410 nm.

### *2.5.7. Determination of kinetic parameters of PHPT1*

Dephosphorylation assays were carried out following the general procedure above except for the

concentration of Sox-H4P (1, 2, 5, 10, 20, 30, 50, and 70 μM). The raw fluorescence data (AFU) were converted to the concentration of the remaining Sox-H4P probe (μM) using the relationship from Figure 1C and 1D. Using the software Origin®, the data were plotted and fitted for Exponential Decay 2 function $(y = A_1 \times \exp(-x/t_1) + A_2 \times \exp(-x/t_2) + y_0)$, in which the *x* axis is time and the *y* axis is the probe concentration. The initial reaction rates were calculated using first derivative at initial time point $(dy/dx|_{x=0} = -A_1/t_1 - A_2/t_2)$. The initial rates and the probe concentrations were fitted for the Michaelis-Menten equation $(y = V_{max} \times x/(K_M + x))$ to obtain the kinetic parameters ($V_{max}$, $K_M$, and $k_{cat}$).

### *2.5.8. PHPT1 Inhibition Assays*

Dephosphorylation assays were carried out following the general procedure with some modifications. Each of common phosphatase inhibitors (sodium fluoride, sodium orthovanadate, *β*-glycerophosphate, sodium pyrophosphate, or imidazole, final concentration of 1 mM) or Phosphatase Inhibitor Cocktail III (Sigma-Aldrich, Catalog No.: P0044, final concentration 1% v/v) was added to separate assay wells without the addition of PHPT1. The fluorescence was measured first to see the interference effect of the inhibitor to the probe fluorescence. In case where the fluorescence was diminished, additional $MgCl_2$ was added to wells until the fluorescence were readjusted to the original fluorescence of Sox-H4P. Typically, additional 1 mM of $MgCl_2$ (final 21 mM) was enough for the fluorescence to return. Then, PHPT1 (final 100 nM) was added and the dephosphorylation reaction was monitored following the general procedure. To confirm the enzyme inhibition, the reaction mixture was also analyzed with HPLC at the end of the reaction.

### *2.5.9. Expression and purification of recombinant proteins*

Expression and purification of recombinant proteins were carried out following the literature[16]. BL21(DE3) Chemically Competent *E. coli* (Invitrogen, Catalog No.: C600003) was used as host, and PHPT1-$His_6$ (pET21a(+) derivative containing PHPT1 from *Homo sapiens*) was used as plasmid.

#### *2.5.9.1. Cell lysis*

Cell pelet was re-suspened in 25 mM Tris, 200 mM NaCl, 2 mM PMSF, pH 7.5 buffer and disrupted with tip-sonicator (5 pulse, 10 pause, 40% amplitude). The lysate was centrifugated at 4000 g for 30 min at 4°C and the supernant was purified by Ni-NTA affinity chromatography.

#### *2.5.9.2. Ni-NTA protein affinity purification*

$His_6$-tagged proteins were purified with HisPur Ni-NTA Resin (Fisher Scientific, Catalog No.: 88223) using standard purification protocol according to manufacturer's recommendation. Buffer compositions are basically 25 mM Tris/HCl and 200 mM NaCl at pH 7.5 for common, and additional 20 mM imidazole for equilibration and first wash buffer, 50 mM imidazole for second wash buffer, and 200 mM imidazole for elution buffer. The purified protien was analyzed by SDS-PAGE and the concentration was determined with Bradford method after dialysis to remove excess imidazole.

- **SDS-PAGE images by Coomassie blue staining**

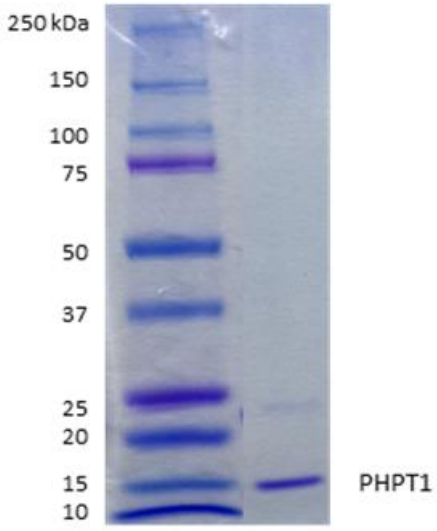


#### *2.5.10. Preparation of HeLa cell lysate*

HeLa cells were kind gifts from the Rhee lab and Ryu lab (UNIST, Ulsan, South Korea) and cultured in 20 mL Dulbecco's modified Eagle's medium (DMEM, Welgene) supplemented with 10% fetal bovine serum (FBS, Welgene) and 1% penicillin-streptomycin (Gibco) in 75 $cm^2$ flask. Growth medium were removed from confluent monolayer of cells. Cells were washed with 3 mL Dulbecco's phosphate-buffered saline (DPBS, Welgene) prior to incubation with 2 mL 0.25% trypsin-EDTA (Gibco) for 5 min at RT. Reaction was quenched with 8 mL DMEM supplemented with 10% FBS. Suspended cells were transferred to a 15 mL conical tube and centrifuged at 4°C for 3 min at 1000 rpm. The resulting cell pellet were washed twice with 5 mL DMEM and lysed in 500 μL lysis buffer (50 mM Tris, pH 7.5, 150 mM NaCl, 1 mM PMSF, 0.5 mM DTT, 1 mM EGTA) using a water-bath sonicator (3 sec on and 3 sec off for 6 min at an amplitude of 85%). Cleared lysates were obtained by centrifugation at 4°C for 5 min at 13000 rpm.

### *2.5.11. Experimental procedure and spectroscopic data for Sox-based probes*

N-terminal acetylated peptides were synthesized following general SPPS protocol.

#### *2.5.11.1. Synthesis of Sox-Br*

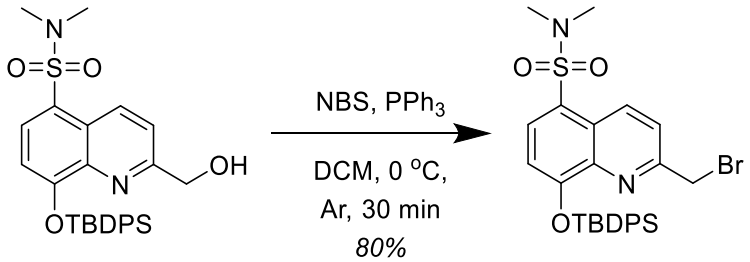


**Sox-OH** **Sox-Br**

8-((tert-butyldiphenylsilyl)oxy)-2-(hydroxymethyl)-N,N-dimethylquinoline-5-sulfonamide (Sox-OH) was prepared according to the published procedure with minor modifications.[17] To the solution of Sox-OH (200 mg, 0.38 mmol) in dry dichloromethane (1 mL) was added *N*-bromosuccinimide (140 mg, 0.77 mmol) at 0°C under Ar. Triphenylphosphine (191 mg, 0.73 mmol) was dissolved in dry dichloromethane (1 mL) in separate vessel and added to the mixture slowly. After reaction mixture was stirred for 30 min at same temperature, it was diluted with diethyl ether. The organic layers were washed with saturated ammonium chloride and brine, dried over magnesium sulfate anhydrous, filtered, and concentrated *in vacuo* to give crude products. Flash column chromatography on Florisil (100-200 mesh, 10 % ethyl acetate in hexane) gave Sox-Br (179 mg, 80%) as a colorless oil. All analytical data are consistent with the literature.

**TLC** $R_f$ (33% ethyl acetate in hexane) = 0.7, visible under 254 nm UV light.

**$^1$H NMR** (400 MHz, $CDCl_3$) δ (ppm) 8.93 (d, *J* = 9.0 Hz, 1H), 8.02 (d, *J* = 8.3 Hz, 1H), 7.73 (d, *J* = 6.6 Hz, 4H), 7.51 (d, *J* = 9.0 Hz, 1H), 7.39 – 7.27 (m, 6H), 7.15 (d, *J* = 8.3 Hz, 1H), 4.13 (s, 2H), 2.72 (s, 6H), 1.17 (s, 9H).

**$^{13}$C NMR** (101 MHz, $CDCl_3$) δ 157.15, 155.42, 140.29, 134.93, 134.59, 133.37, 132.42, 129.65, 127.58, 125.36, 123.81, 122.72, 115.75, 37.33, 32.71, 26.58, 20.17.

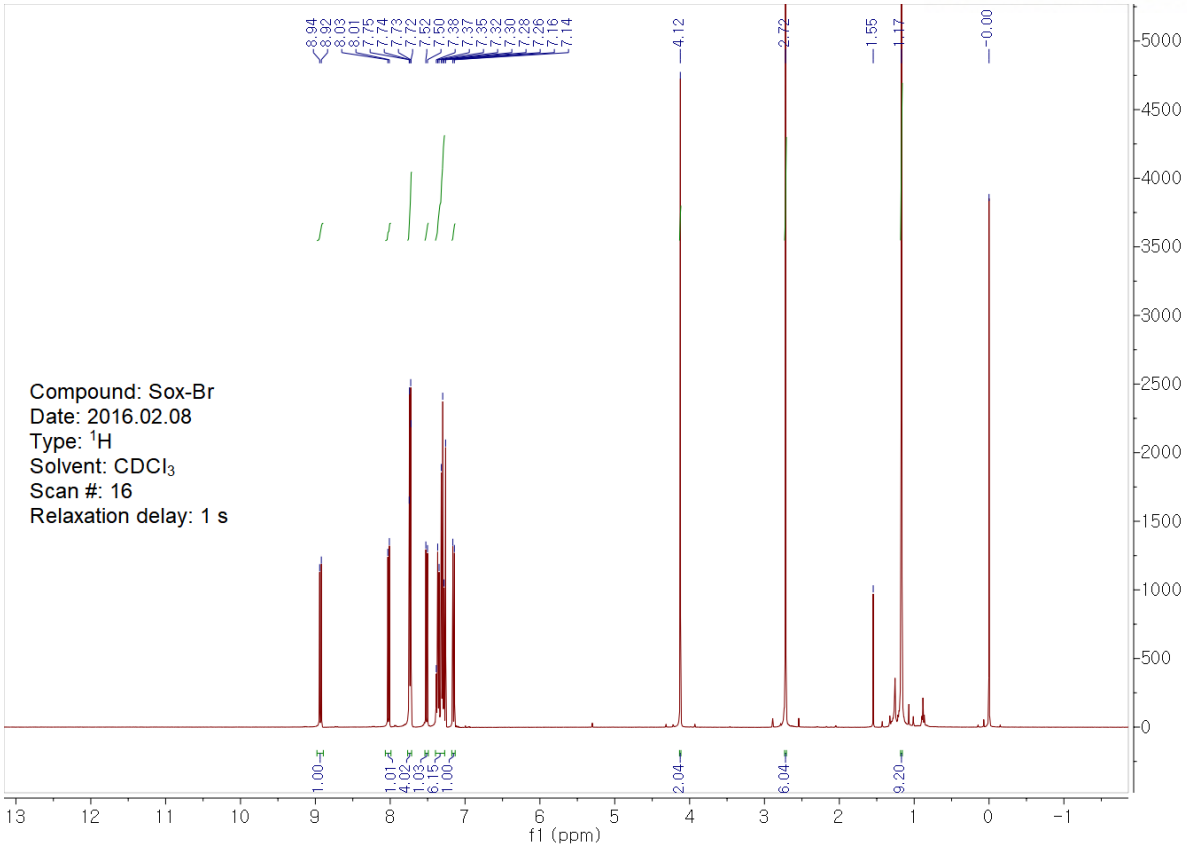


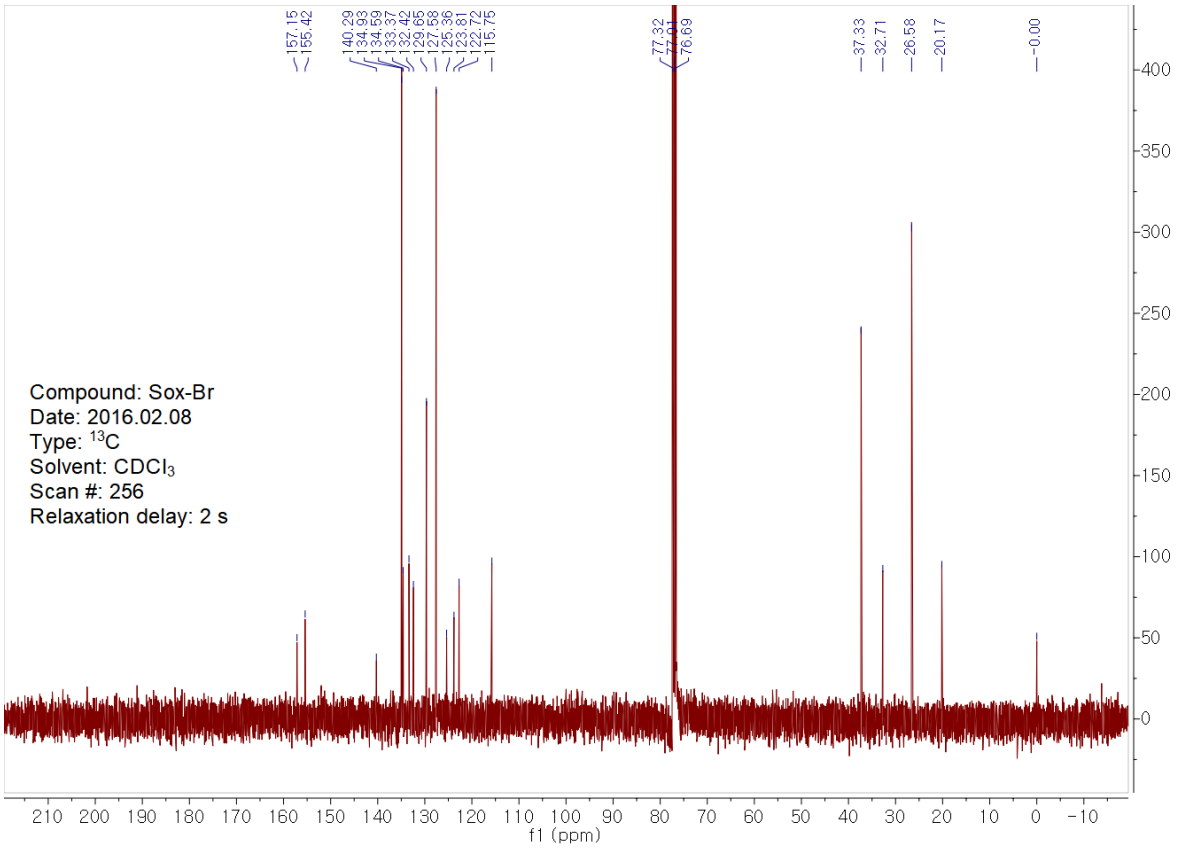

#### *2.5.11.2. On-resin alkylation of peptides with Sox-Br*

Preparation of Sox-Br and Sox alkylation to Cys was carried out following the procedure in the literature with slight modifications.[3,6] The modified alkylation procedure is given below.

The resin with fully protected peptide (20 μmol) was swollen in $CH_2Cl_2$ (5 × 5 min × 2 mL) with $N_2$ bubbling and drained. To the resin-bound peptide was added 2 mL of 1% TFA and 5% TIS in $CH_2Cl_2$ for selective Mmt deprotection and the mixture was bubbled with $N_2$ for 20 min. Yellow color appeared immediately. The Mmt deprotection was repeated (usually more than 6 times) until no more yellow color was observed. Following the deprotection, the resin was washed (5 × $CH_2Cl_2$ then 5 × anhydrous DMF). To activate the thiol on Cys, 17.3 μL (100 μmol) of DIPEA dissolved in 430 μL of anhydrous DMF was added to the resin. After 2 min, Sox-Br (23.3 mg, 40 μmol) in 210 μL of anhydrous DMF was added to the resin and it was bubbled with $N_2$ overnight (12 hr) in the dark. Following the alkylation, the resin was washed (5 × DMF, 5 × $CH_2Cl_2$, 5 × MeOH, 5 × $CH_2Cl_2$) and proceeded to the peptide cleavage and purification as normal.

#### *2.5.11.3. Chemical phosphorylation on histidine residue of Sox-H4*

The Sox-H4 (1 mM) were specifically phosphorylated on the histidine residue using 500 equiv. of potassium phosphoramidate (PPA) in 1 mL of phosphate buffer (pH 8) to yield the corresponding Sox-H4P peptides. Reaction was monitored by analytical HPLC (C18, 1.0 mL/min, 23-25B over 8 min). Typically, 80~90% of Sox-H4 was phosphorylated to Sox-H4P within 8 hr. Crude reaction mixture was purified by semi-preparative HPLC (C18, 2.5 mL/min, 23-25B over 20 min) and the collected fractions were immediately basified to pH 9 with ammonium hydroxide and evaporated to remove the solvent. Purified Sox-H4P stock solution was quantified with HPLC and stored under -80°C. With aid of LC-MS/MS (ETD), C-Sox position and pHis were validated (see below for the spectra).

### *2.5.12. Analytical data for Sox-H4 and Sox-H4P series.*

#### *2.5.12.1. List of synthesized Sox-H4 and Sox-H4P peptides.*

| ENTRY | COMPOUND | PEPTIDE SEQUENCE | ANALYTICAL DATA |
|---|---|---|---|
| (-3) | Sox-H4(-3) | Ac-GG(CSox)KRHRKVL-$NH_2$ | HPLC, ESI-MS |
| | Sox-H4P(-3) | Ac-GG(CSox)KRpHRKVL-$NH_2$ | HPLC, ESI-MS, MS/MS |
| (-2) | Sox-H4(-2) | Ac-GGA(CSox)RHRKVL-$NH_2$ | HPLC, ESI-MS |
| | Sox-H4P(-2) | Ac-GGA(CSox)RpHRKVL-$NH_2$ | HPLC, ESI-MS, MS/MS |
| (-1) | Sox-H4(-1) | Ac-GGAK(CSox) HRKVL-$NH_2$ | HPLC, ESI-MS |
| | Sox-H4P(-1) | Ac-GGAK(CSox) pHRKVL-$NH_2$ | HPLC, ESI-MS, MS/MS |
| (+1) | Sox-H4(+1) | Ac-GGAKRH (CSox)KVL-$NH_2$ | HPLC, ESI-MS |
| | Sox-H4P(+1) | Ac-GGAKRpH (CSox)KVL-$NH_2$ | HPLC, ESI-MS, MS/MS |
| (+2) | Sox-H4(+2) | Ac-GGAKRHR(CSox)VL-$NH_2$ | HPLC, ESI-MS |
| | Sox-H4P(+2) | Ac-GGAKRpHR(CSox)VL-$NH_2$ | HPLC, ESI-MS, MS/MS |
| (+3) | Sox-H4(+3) | Ac-GGAKRHRK(CSox)L-$NH_2$ | HPLC, ESI-MS |
| | Sox-H4P(+3) | Ac-GGAKRpHRK(CSox)L-$NH_2$ | HPLC, ESI-MS, MS/MS |

#### *2.5.12.2. HPLC and LC-MS/MS data*

RP-HPLC method: C18, 1 mL/min, 0-70B over 8 min, detector at 254 nm (referenced to 360 nm)

- **Sox-H4(-3): Ac-GGC(Sox)KRHRKVL-NH$_2$**

**HPLC**

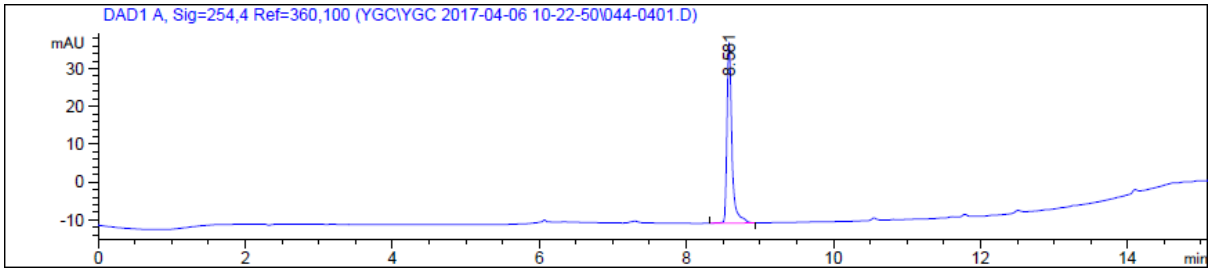


**ESI-MS (HR-MS)**: Calculated m/z $[M+2H]^{+2}$: 729.8821, Observed m/z $[M+2H]^{+2}$: 729.8816.

- **Sox-H4P(-3): Ac-GGC(Sox)KRpHRKVL-NH$_2$**

**HPLC**

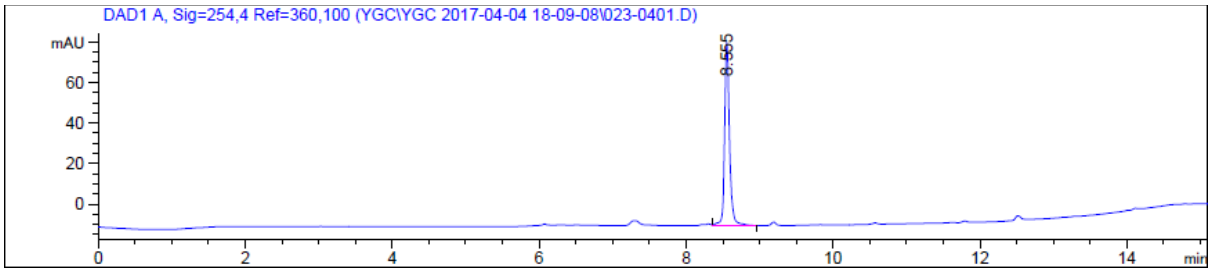


**ESI-MS (HR-MS)**: a. Calculated m/z $[M+2H]^{+2}$: 729.8821, Observed m/z $[M+2H]^{+2}$: 729.8820. b. Calculated m/z $[pM+2H]^{+2}$: 769.8653, Observed m/z $[pM+2H]^{+2}$: 769.8652. c. Calculated m/z $[pM+H+K]^{+2}$: 788.8432, Observed m/z $[pM+H+K]^{+2}$: 788.8431. d. Calculated m/z $[pM+2K]^{+2}$: 807.8211, Observed m/z $[pM+2K]^{+2}$: 807.8208

**LC-MS/MS (ETD)**

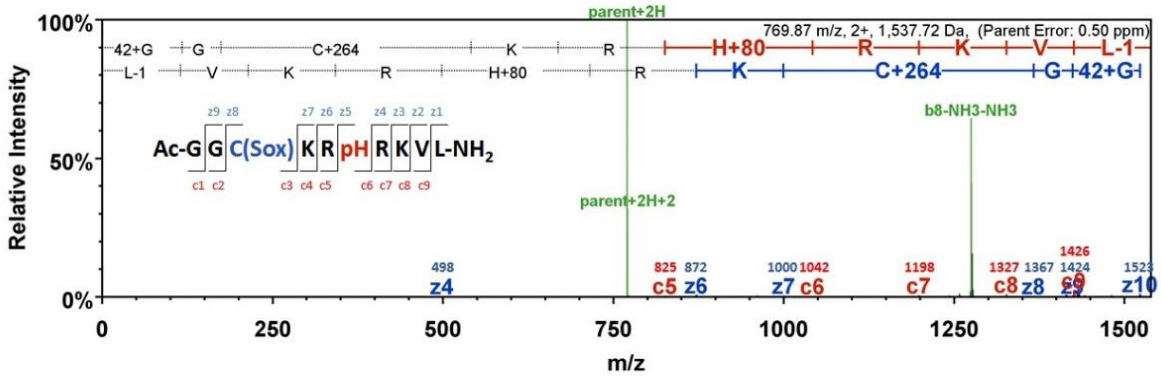


**LC-MS/MS (ETD) (zoomed-in spectrum)**

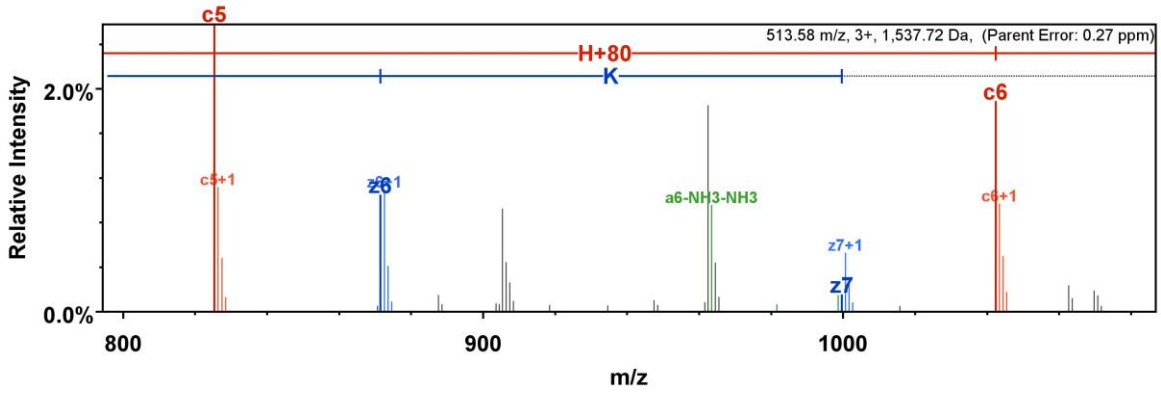

- **Sox-H4(-2): Ac-GGAC(Sox)RHRKVL-NH$_2$**

**HPLC**

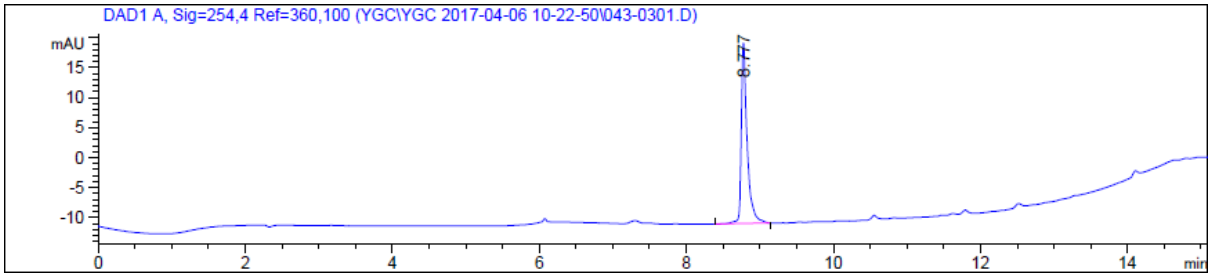


**ESI-MS (HR-MS)**: Calculated m/z $[M+2H]^{+2}$: 701.3532, Observed m/z $[M+2H]^{+2}$: 701.3545.

- **Sox-H4P(-2): Ac-GGAC(Sox)RpHRKVL-NH$_2$**

**HPLC**

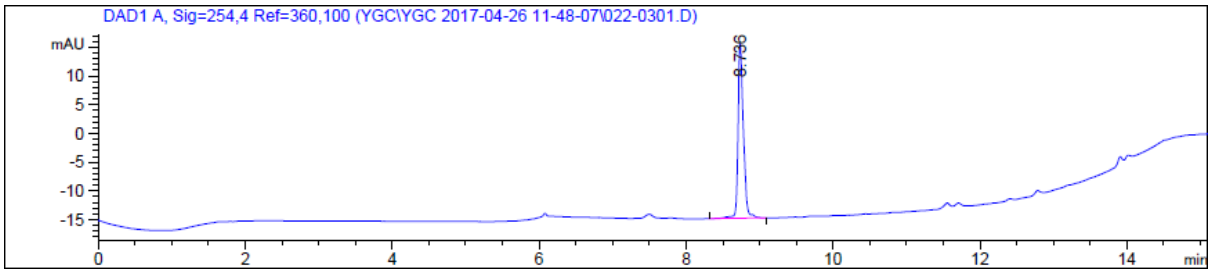


**ESI-MS (HR-MS)**: a. Calculated m/z $[M+2H]^{+2}$: 701.3532, Observed m/z $[M+2H]^{+2}$: 701.3534. b. Calculated m/z $[pM+2H]^{+2}$: 741.3363, Observed m/z $[pM+2H]^{+2}$: 741.3367. c. Calculated m/z $[pM+H+K]^{+2}$: 760.3143, Observed m/z $[pM+H+K]^{+2}$: 760.3144. d. Calculated m/z $[pM+2K]^{+2}$: 779.2922, Observed m/z $[pM+2K]^{+2}$: 779.2919.

**LC-MS/MS (ETD)**

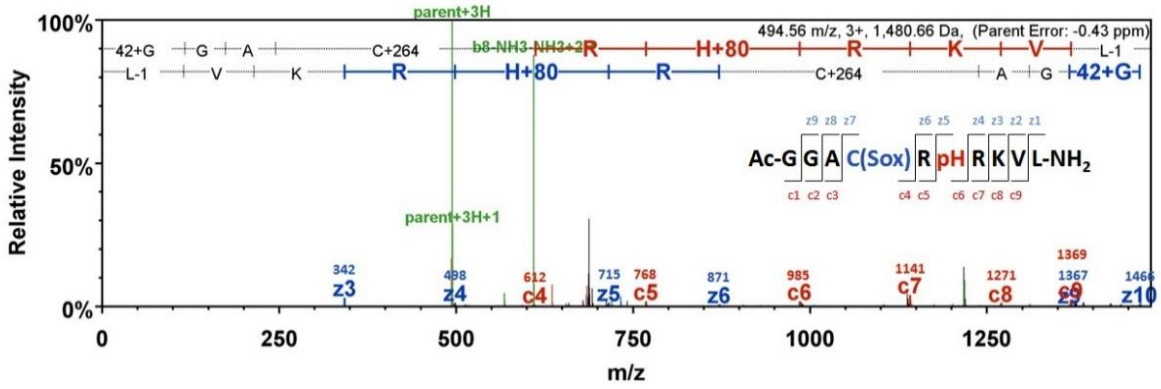


**LC-MS/MS (ETD) (zoomed-in spectrum)**

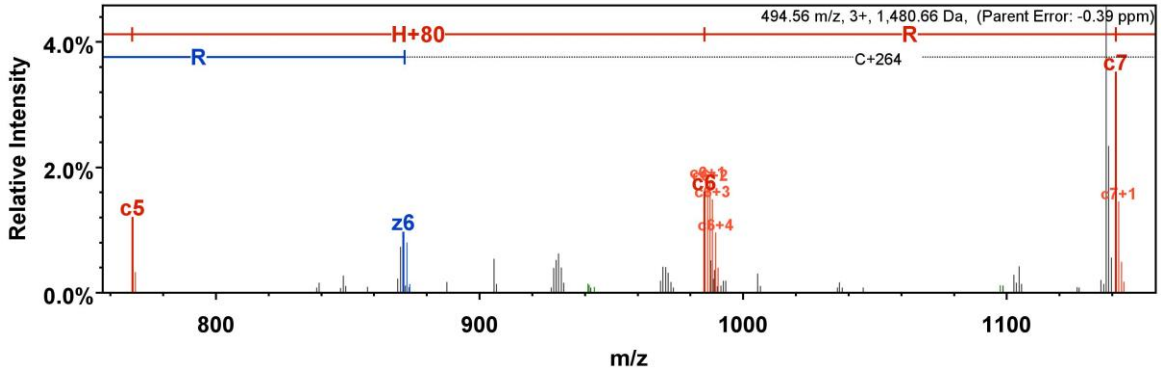


**LC-MS/MS (CID)**

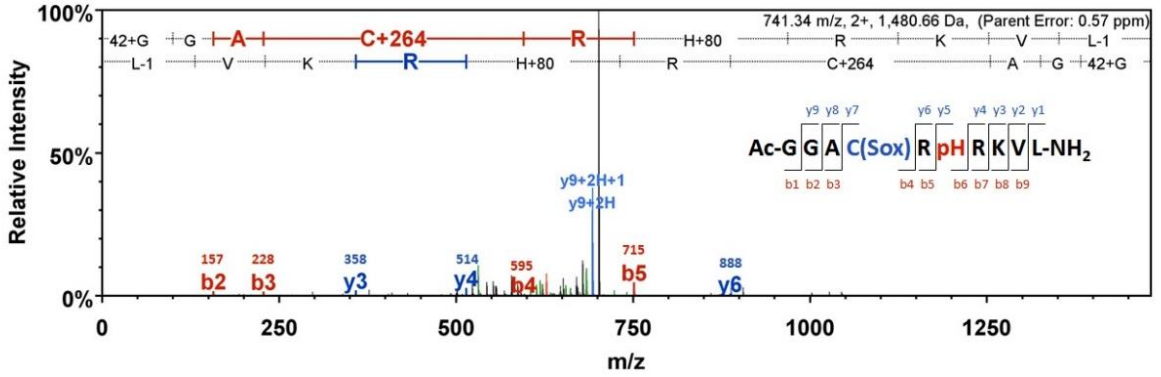

- **Sox-H4(-1): Ac-GGAKC(Sox)HRKVL-NH$_2$**

**HPLC**

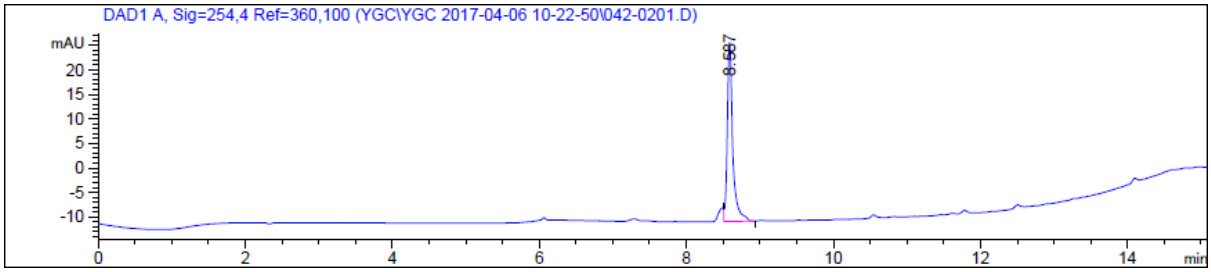


**ESI-MS (HR-MS)**: Calculated m/z $[M+2H]^{+2}$: 687.3501, Observed m/z $[M+2H]^{+2}$: 687.3508.

- **Sox-H4P(-1): Ac-GGAKC(Sox)pHRKVL-NH$_2$**

**HPLC**

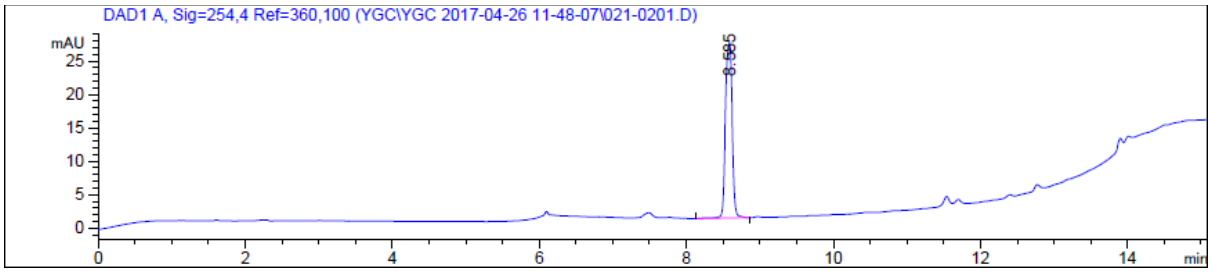


**ESI-MS (HR-MS)**: a. Calculated m/z $[M+2H]^{+2}$: 687.3501, Observed m/z $[M+2H]^{+2}$: 687.3497. b. Calculated m/z $[pM+2H]^{+2}$: 727.3333, Observed m/z $[pM+2H]^{+2}$: 727.3332. c. Calculated m/z $[pM+H+Na]^{+2}$: 738.3242, Observed m/z $[pM+H+Na]^{+2}$: 738.3234. d. Calculated m/z $[M+2Na]^{+2}$: 749.3152, Observed m/z $[pM+H+Na]^{+2}$: 749.3141.

**LC-MS/MS (ETD)**

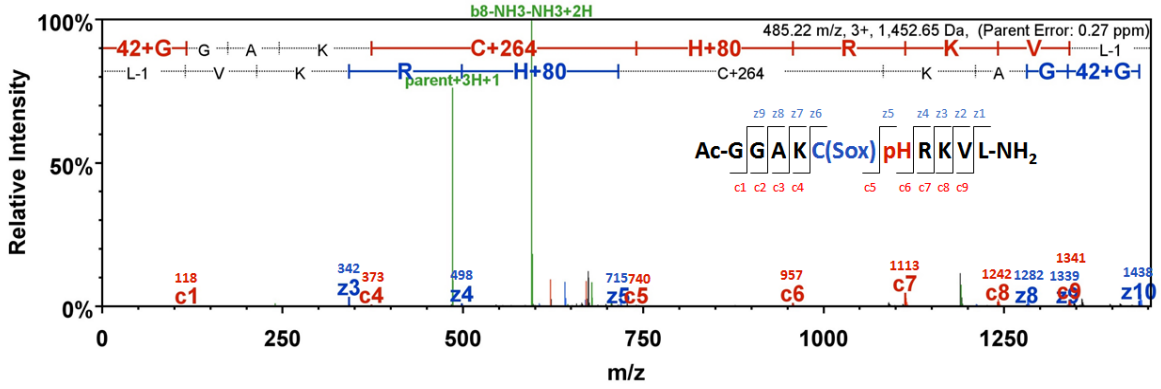


**LC-MS/MS (ETD) (zoomed-in spectrum)**

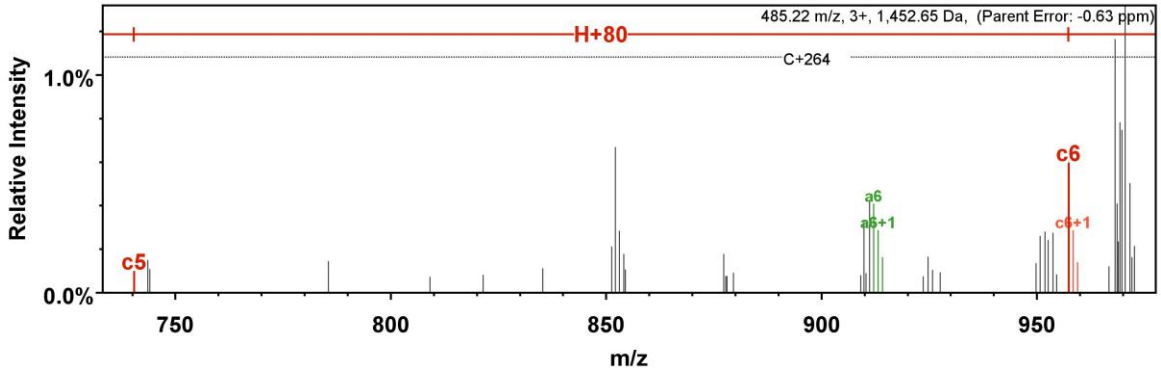

- **Sox-H4(+1): Ac-GGAKRHC(Sox)KVL-$NH_2$**

**HPLC**

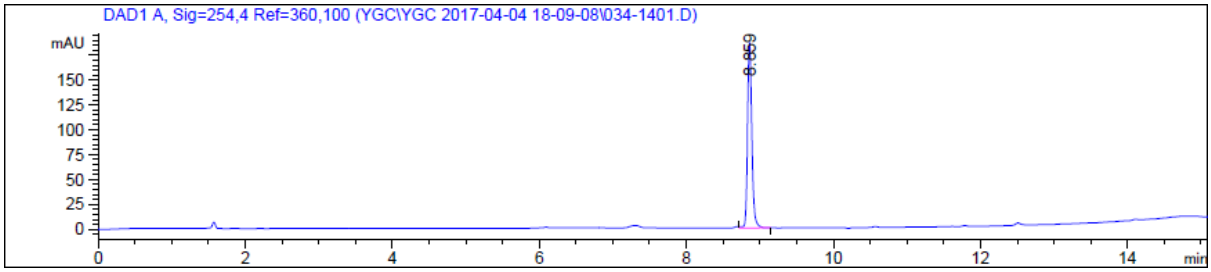


**ESI-MS (HR-MS)**: Calculated m/z $[M+2H]^{+2}$: 687.3501, Observed m/z $[M+2H]^{+2}$: 687.3503.

- **Sox-H4P(+1): Ac-GGAKRpHC(Sox)KVL-$NH_2$**

**HPLC**

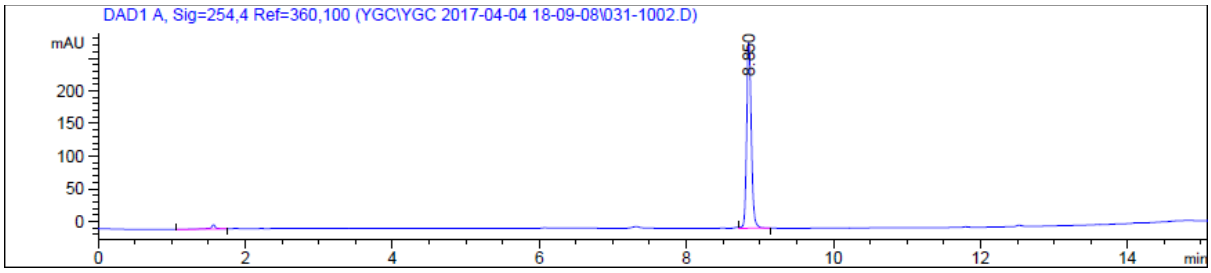


**ESI-MS (HR-MS)**: a. Calculated m/z $[M+2H]^{+2}$: 687.3501, Observed m/z $[M+2H]^{+2}$: 687.3496. b. Calculated m/z $[pM+2H]^{+2}$: 727.3333, Observed m/z $[pM+2H]^{+2}$: 727.3337.

**LC-MS/MS (ETD)**

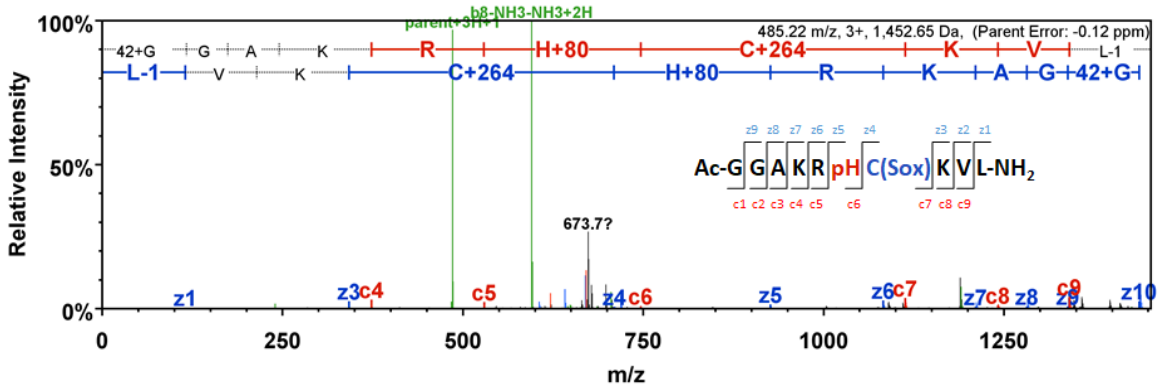


**LC-MS/MS (ETD) (zoomed-in spectrum)**

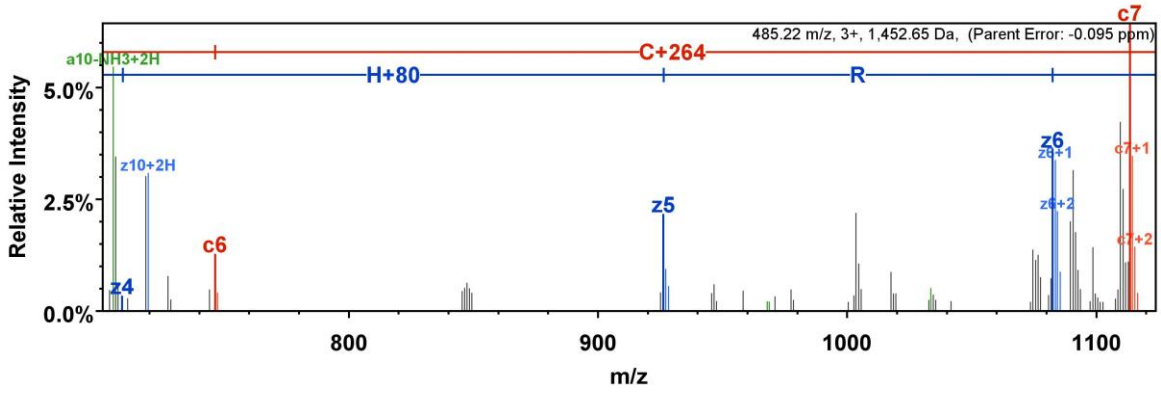

- **Sox-H4(+2): Ac-GGAKRHRC(Sox)VL-$NH_2$**

**HPLC**

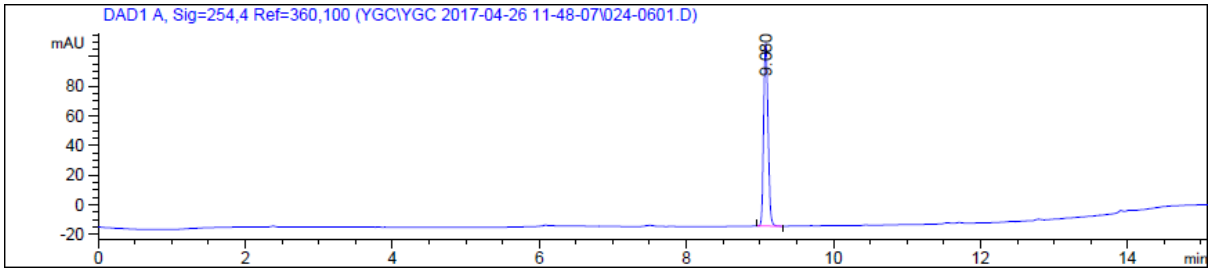


**ESI-MS (HR-MS)**: Calculated m/z $[M+2H]^{+2}$: 701.3532, Observed m/z $[M+2H]^{+2}$: 701.3532.

- **Sox-H4P(+2): Ac-GGAKRpHRC(Sox)VL-$NH_2$**

**HPLC**

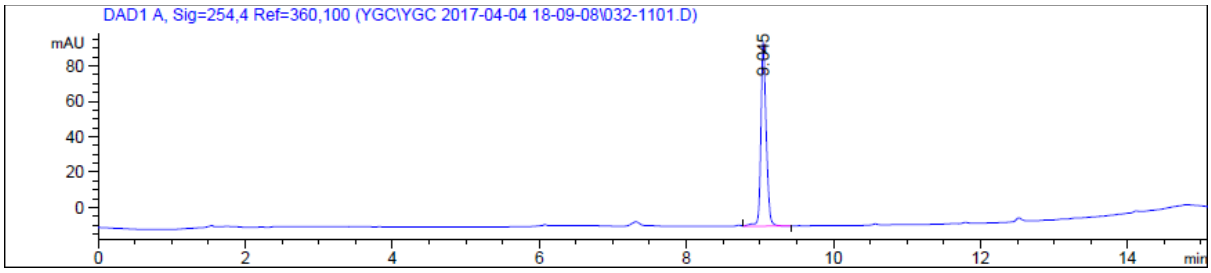


**ESI-MS (HR-MS)**: a. Calculated m/z $[M+2H]^{+2}$: 701.3532, Observed m/z $[M+2H]^{+2}$: 701.3525. b. Calculated m/z $[pM+2H]^{+2}$: 741.3363, Observed m/z $[pM+2H]^{+2}$: 741.3363. c. Calculated m/z $[pM+H+Na]^{+2}$: 752.3275, Observed m/z $[pM+H+Na]^{+2}$: 752.3267.

**LC-MS/MS (ETD)**

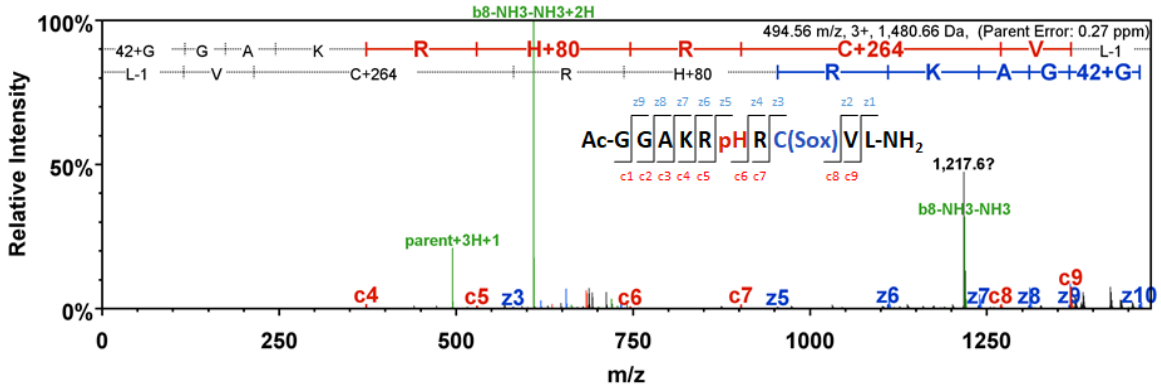


**LC-MS/MS (ETD) (zoomed-in spectrum)**

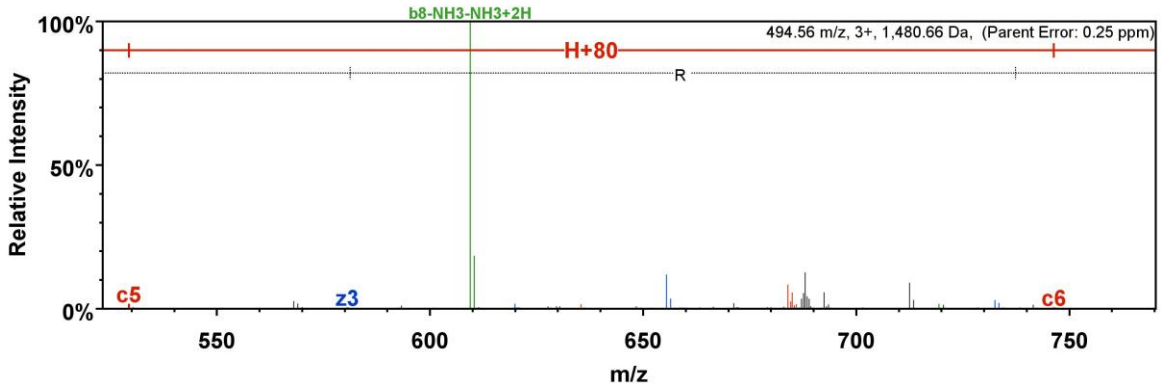

- **Sox-H4(+3): Ac-GGAKRHRKC(Sox)L-$NH_2$**

**HPLC**

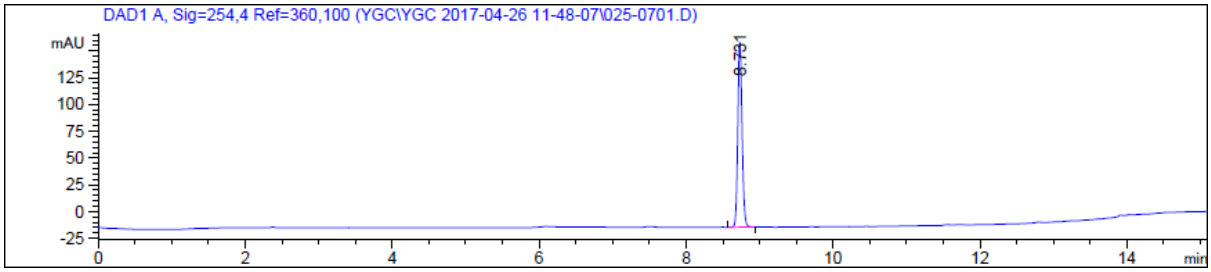


**ESI-MS (HR-MS)**: Calculated m/z $[M+2H]^{+2}$: 715.8664, Observed m/z $[M+2H]^{+2}$: 715.8667.

- **Sox-H4P(+3): Ac-GGAKRpHRKC(Sox)L-$NH_2$**

**HPLC**

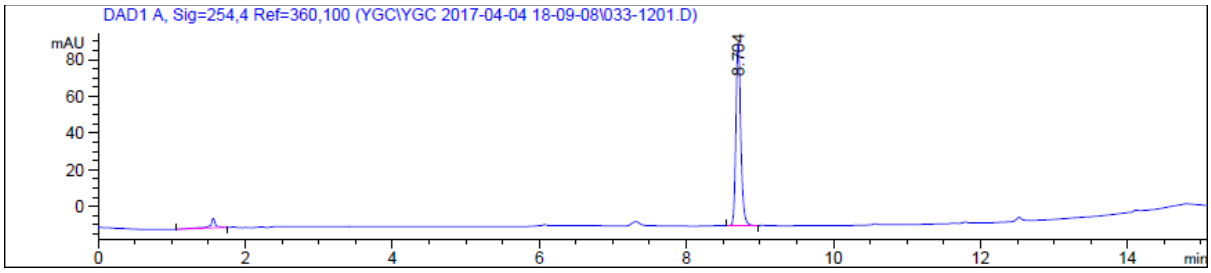


**ESI-MS (HR-MS)**: a. Calculated m/z $[M+2H]^{+2}$: 715.8664, Observed m/z $[M+2H]^{+2}$: 715.8656. b. Calculated m/z $[pM+2H]^{+2}$: 755.8496, Observed m/z $[pM+2H]^{+2}$: 755.8488. c. Calculated m/z $[pM+H+Na]^{+2}$: 766.8406, Observed m/z $[pM+H+Na]^{+2}$: 766.8400.

**LC-MS/MS (ETD)**

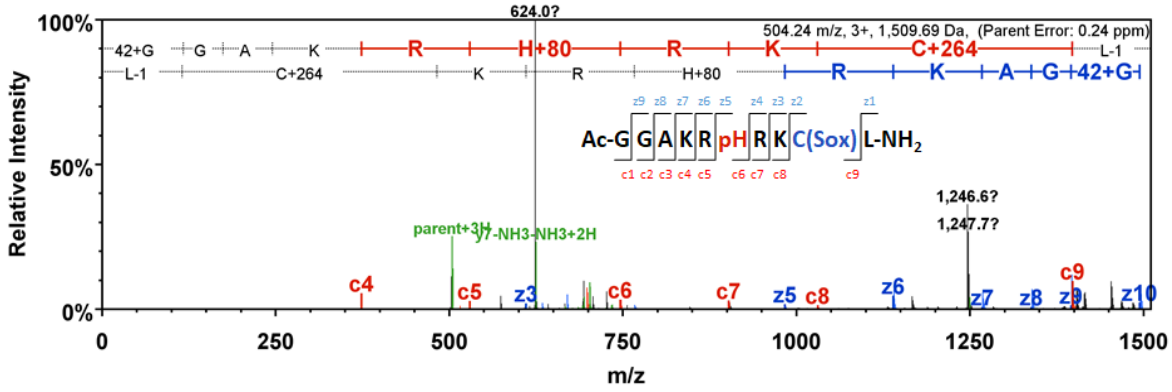


**LC-MS/MS (ETD) (zoomed-in spectrum)**

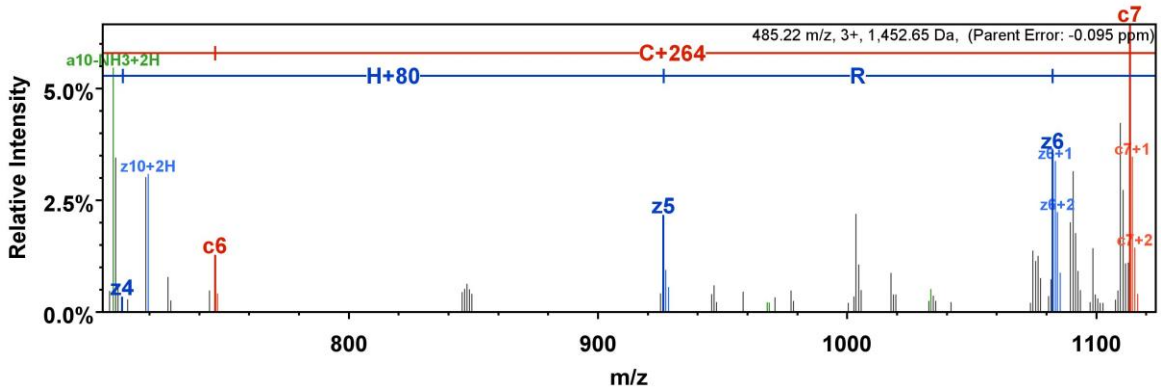

### *2.5.12.3. UV absorption and emission spectra of Sox-H4P*

10 μM of Sox-H4P(-2) with 20 mM of $MgCl_2$ in pH 7.5 TBS.

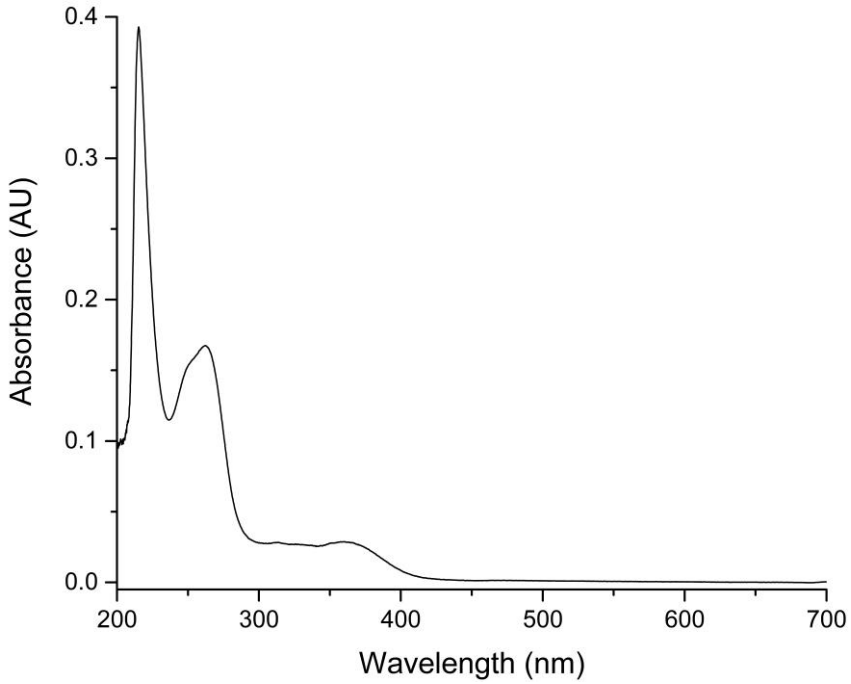


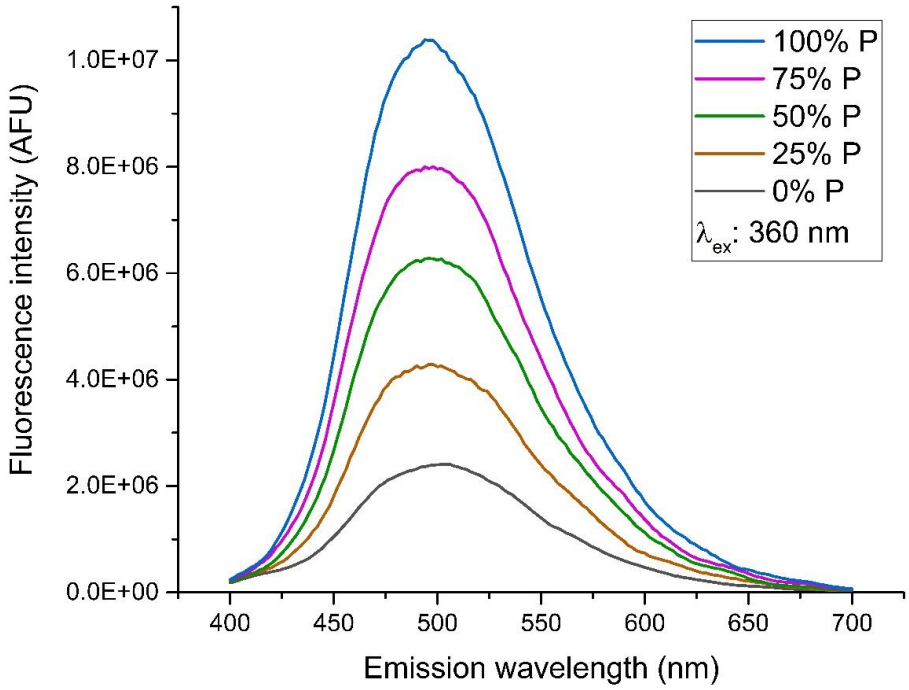

### *2.5.13. Experimental procedure and spectroscopic data for naphthalimide-based probes*

#### *2.5.13.1. Synthesis of HN-P*

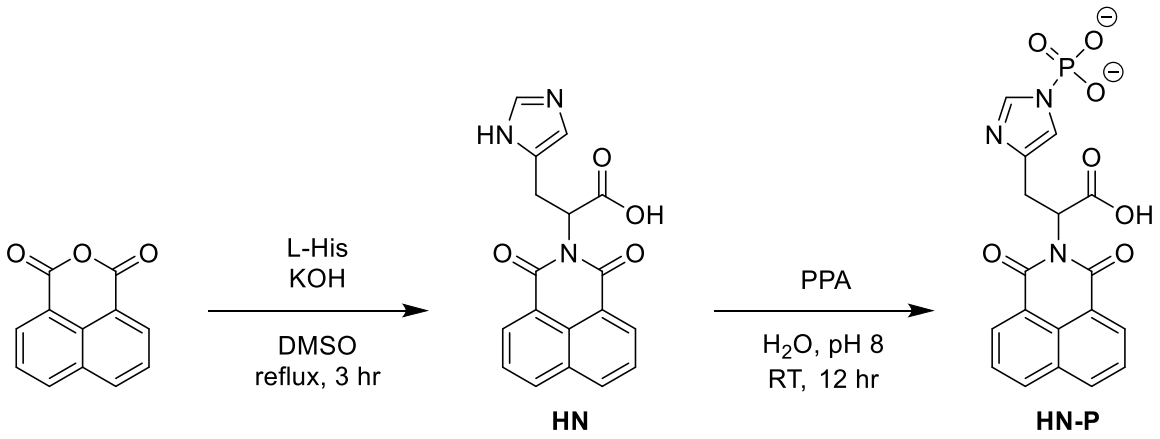


HN was prepared according to the published procedure.[10] To the solution of HN (20 mg, 60 μmol) in pH 8 water (5 mL) was added potassium phosphoramidate (162 mg, 1.2 mmol) at RT. The reaction mixture was stirred for 8 hr and set pH as 9. The solvent was removed by rotary evaporator and re-dissolved in methanol for removal of excess phosphates. The solvent was removed by rotary evaporator and re-dissolved in pH 9 water, following the purification *via* semi-preparative HPLC (C18, 2.5 mL/min, 30-31B over 20 min). After lyophilizing, HN-P was yielded as a white solid.

**TLC** $R_f$ (4% water and 26% methanol in chloroform) = 0.23 for HN and baseline for HN-P, visible under both 254 and 360 nm UV light.

**$^1$H NMR** (400 MHz, $CDCl_3$) δ (ppm) 8.51 (s, 1H), 8.37 (d, *J* = 7.4 Hz, 2H), 8.22 (d, *J* = 7.9, 2H), 7.69 (dd, *J* = 8.2, 7.4 Hz, 2H), 7.15 (s, 1H), 5.99 (dd, *J* = 9.2, 5.4 Hz, 1H), 3.72 (dd, *J* = 15.7, 5.4 Hz, 1H), 3.50 (dd, *J* = 15.7, 9.2 Hz, 1H) for HN. 8.51 – 8.41 (m, 2H), 8.35 (d, *J* = 8.2 Hz, 2H), 7.77 (t, *J* = 7.8 Hz, 2H), 7.06 (s, 1H), 5.71 (dd, *J* = 10.0, 4.9 Hz, 1H), 3.62 (dd, *J* = 15.9, 5.5 Hz, 1H), 3.47 (dd, *J* = 15.5, 10.2 Hz, 1H) for HN-P.

**MALDI-TOF MS** Calculated m/z $[M+H]^+$: 336.0979, Observed m/z $[M+H]^+$: 336.6895 for HN, 416.0642, Observed m/z $[M+H]^+$: 416.4847 for HN-P.

### *2.5.13.2. Synthesis of HMeN-P*

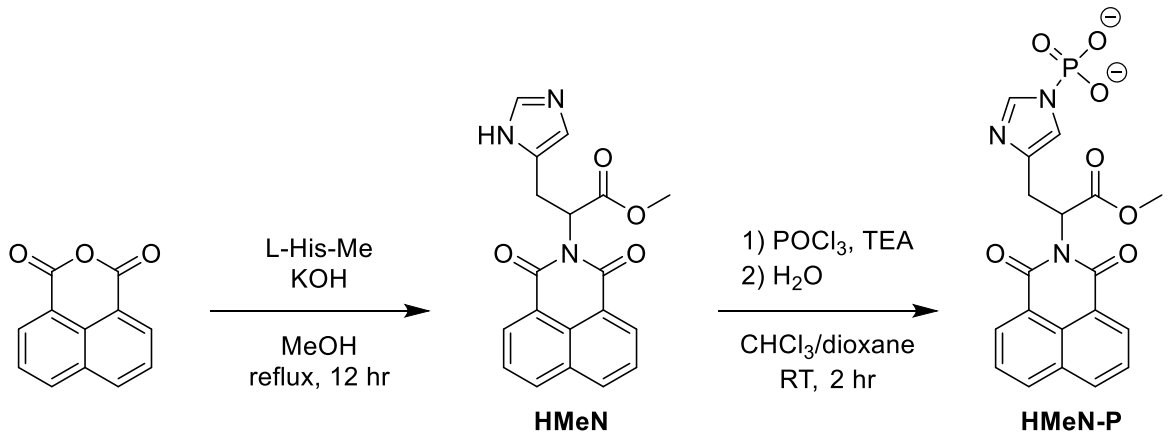


HMeN was prepared according to the published procedure with modification of the solvent to methanol from dimethyl sulfoxide.[10] To the solution of HMeN (16.8 mg, 48 μmol) in chloroform (3 mL) and dioxane (1 mL) was added triethylamine (134 μL, 0.96 mmol) at RT. Phosphoryl chloride (22.3 μL, 0.24 mmol) was slowly added to the reaction mixture. After 1 hr of stirring, water (1 mL) was added and the reaction mixture was stirred for additional 1 hr. The solvent was removed by rotary evaporator, and the residue was re-dissolved in water, following wash with chloroform. The aqueous layer was basified by ammonia to prevent unwanted dephosphorylation.

**TLC** $R_f$ (4% water and 26% methanol in chloroform) = 0.8 for HMeN, 0.6 for the intermediate, and less than 0.1 for HMeN-P, visible under both 254 and 360 nm UV light.

**$^1$H NMR** (400 MHz, $CDCl_3$) δ (ppm) 8.74 (s, 1H), 8.55 (d, *J* = 8.4 Hz, 2H), 8.43 (d, *J* = 7.4 Hz, 2H), 7.88 – 7.83 (m, 2H), 7.30 (s, 1H), 6.03 (dd, *J* = 9.3, 5.1 Hz, 1H), 3.80 – 3.75 (m, 1H), 3.74 (s, 3H), 3.58 (dd, *J* = 15.6, 9.3 Hz, 1H) for HMeN.

**MALDI-TOF MS** Calculated m/z $[M+H]^+$: 350.1135, Observed m/z $[M+H]^+$: 350.6048 for HMeN, Calculated m/z $[M+H]^+$: 430.0799, Observed m/z $[M+H]^+$: 430.4128 for HMeN-P.

### *2.5.13.3. Synthesis of HMeBN-P*

HMeBN was prepared according to the published procedure with minor modifications.[8] Instead of precipitation, the crude mixture was purified by extraction with chloroform and saturated ammonium chloride. The organic layers were washed with brine, dried over magnesium sulfate anhydrous, filtered, and concentrated *in vacuo* to give HMeBN (80% yield) as a white solid. Phosphorylation of HMeBN followed same protocol as 2.5.13.2.

**TLC $R_f$** (4% water and 26% methanol in chloroform) = 0.77 for HMeBN, 0.56 for the intermediate, and less than 0.1 for HMeBN-P, visible under both 254 and 360 nm UV light.

**$^1$H NMR** (400 MHz, $CDCl_3$) δ (ppm) 8.61 – 8.54 (m, 2H), 8.34 (d, *J* = 7.9 Hz, 1H), 8.02 (d, *J* = 7.9 Hz, 1H), 7.82 (dd, *J* = 8.4, 7.4 Hz, 1H), 7.44 (s, 1H), 6.75 (s, 1H), 5.95 (dd, *J* = 8.3, 6.1 Hz, 1H), 3.74 (s, 3H), 3.66 (dd, *J* = 15.2, 6.0 Hz, 1H), 3.44 (dd, *J* = 15.2, 8.3 Hz, 1H) for HMeBN. 8.36 – 8.28 (m, 2H), 8.20 (s, 1H), 8.09 (d, *J* = 7.8 Hz, 1H), 7.84 (d, *J* = 7.8 Hz, 1H), 7.69 – 7.63 (m, 1H), 7.06 (s, 1H), 5.91 (dd, *J* = 8.8, 5.7 Hz, 1H), 3.67 (s, 3H), 3.61 (dd, *J* = 16.2, 4.9 Hz, 1H), 3.31 (dd, *J* = 16.1, 9.1 Hz, 1H) for HMeBN-P.

**$^{13}$C NMR** (101 MHz, $CDCl_3$) δ (ppm) 170.41, 163.11, 134.93, 133.69, 132.50, 131.65, 131.15, 130.78, 130.67, 129.10, 128.12, 122.54, 121.66, 53.25, 52.66, 26.37 for HMeBN.

**MALDI-TOF MS** Calculated m/z $[M+H]^+$: 428.0240, Observed m/z $[M+H]^+$: 428.0460 for HMeBN, Calculated m/z $[M+H]^+$: 507.9904, Observed m/z $[M+H]^+$: 508.0083 for HMeBN-P.

#### *2.5.13.4. Excitation and emission spectra of naphthalimide-based probes*

- **HN-P**

Unknown concentration of HN-P in pH 7.5 TBS.

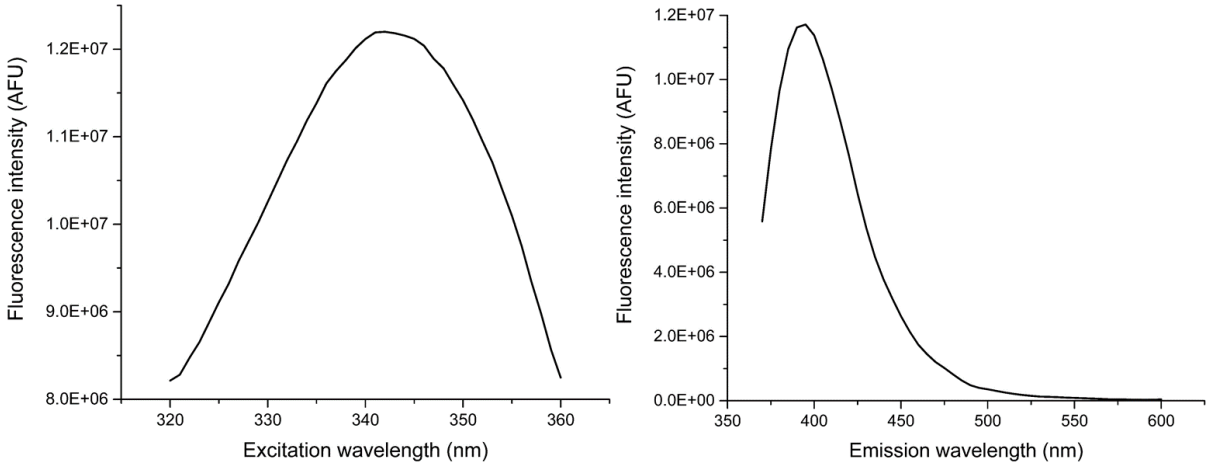


- **HMeN-P**

Unknown concentration of HMeN-P in pH 7.5 TBS.

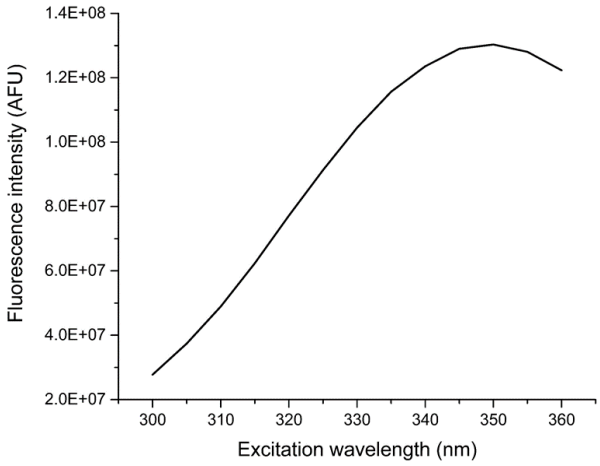


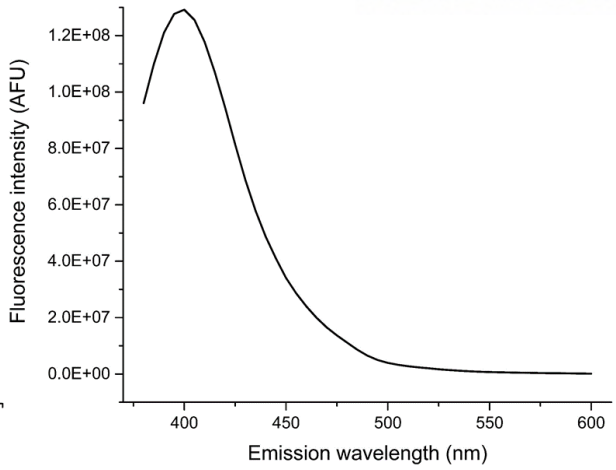


- **HMeBN-P**

Unknown concentration of HMeBN-P in pH 7.5 TBS.

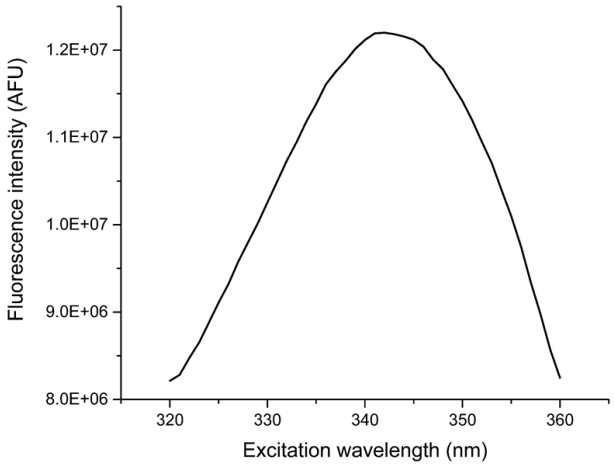


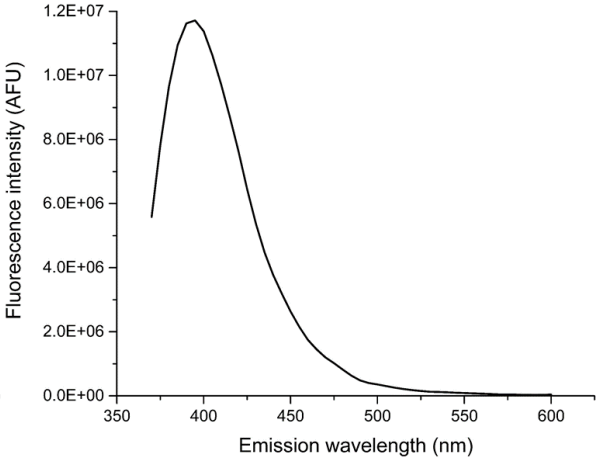

## 2.6. References

[1] Shults, M. D.; Imperiali, B. Versatile fluorescence probes of protein kinase activity. *J. Am. Chem. Soc*. **2003**, *125*, 14248-14249.

[2] Pearce, D. A.; Jotterand, N.; Carrico, I. S.; Imperiali, B. Derivatives of 8-hydroxy-2-methylquinoline are powerful prototypes for zinc sensors in biological systems. *J. Am. Chem. Soc.* **2001**, *123*, 5160–5161.

[3] Luković, E.; González-Vera, J. A.; Imperiali, B. Recognition-domain focused chemosensors: Versatile and efficient reporters of protein kinase activity. *J. Am. Chem. Soc.* **2008**, 12821–12827.

[4] Beck, J. R.; Truong, T.; Stains, C. I. Temporal analysis of PP2A phosphatase activity during insulin stimulation using a direct activity probe. *ACS Chem. Biol.* **2016**, *11*, 3284–3288.

[5] Beck, J. R.; Lawrence, A.; Tung, A. S.; Harris, E. N.; Stains, C. I. Interrogating endogenous protein phosphatase activity with rationally designed chemosensors. *ACS Chem. Biol.* **2016**, *11*, 284–290.

[6] Beck, J. R.; Peterson, L. B.; Imperiali, B.; Stains, C. I. Quantification of protein kinase enzymatic activity in unfractionated cell lysates using CSox-based sensors. *Curr. Protoc. Chem. Biol.* **2014**, *6*, 135–156.

[7] Müller, T.; Rathlev, T; Rosenberg, T. Special cases of non-enzymic transphosphorylation. *Biochim. Biophys. Acta* **1956**, *19*, 563–564.

[8] Lozano-Torres, B.; Galiana, I.; Rovira, M.; Garrido, E.; Chaib, S.; Bernardos, A.; Muñoz-Espín, D.; Serrano, M.; Martínez-Máñez, R.; Sancenón, F. An off-on two-photon fluorescent probe for tracking cell senescence in vivo. *J. Am. Chem. Soc.* **2017**, *139*, 8808–8811.

[9] Zhang, Y.-M.; Zhong, K.-P.; Su, J.-X.; Chen, X.-P.; Yao, H.; Wei, T.-B.; Lin, Q. A novel histidine-functionalized 1,8-naphthalimide-based fluorescent chemosensor for the selective and sensitive detection of $Hg^{2+}$ in water. *New J. Chem.* **2017**, *41*, 3303–3307.

[10] Dong, D.; Cheng, L.; Ma, Y. Interaction of naphthalene anhydride derivative with adenosine triphosphate and the catalytic influence on adenosine triphosphate hydrolysis. *Asian J. Chem.* **2015**, *27*, 261–266.

[11] Dooijewaard, D.; Roossien, F. F.; Robillard, G. T. *Escherichia coli* phosphoenolpyruvate dependent phosphotransferase system. NMR studies of the conformation of HPr and P-HPr and the mechanism of energy coupling. *Biochemistry* **1979**, *18*, 2996–3001.

[12] Burfield, D. R.; Smithers, R. H. Desiccant efficiency in solvent drying. 3. Dipolar aprotic solvents. *J. Org. Chem.* **1978**, *43*(20), 3966-3968.

[13] Still, W. C; Kahn, M.; Mitra, A. Rapid chromatographic technique for preparative separations with moderate resolution. *J. Org. Chem.* **1978**, *43*(14), 2923-2925.

[14] Harris, R. K.; Becker, E. D.; de Menezes, C. S. M.; Goodfellow, R.; Granger, P. NMR nomenclature. Nuclear spin properties and conventions for chemical shifts (IUPAC recommendations 2001). *Pure Appl. Chem.* **2001**, *73*(11), 1795-1818.

[15] Fuhrmann, J.; Subramanian, V.; Thompson, P. R. Synthesis and use of a phosphonate amidine to generate an anti-phosphoarginine-specific antibody. *Angew. Chem. Int. Ed. Engl.* **2015**, *54*(49), 14715–14718.

[16] Ek, P.; Pettersson, G.; Ek, B.; Gong, F.; Li, J. P.; Zetterqvist, Ö. Identification and characterization of a mammalian 14-kDa phosphohistidine phosphatase. *Eur. J. Biochem.* **2002**, *269*(20), 5016-5023.

[17] Shults, M. D.; Pearce, D. A.; Imperiali, B. Modular and tunable chemosensor scaffold for divalent zinc. *J. Am. Chem. Soc.* **2003**, *125*(35), 10591–10597.

## Acknowledgement

First of all, I am grateful to my advisor Prof. Jung-Min Kee. Under his guidance and support, I had advanced in not only academic and experimental capabilities but also humane qualities. Before I joined Prof. Kee's laboratory, I have no knowledge and scholarly interest on chemical biology. Through the lab life, I can grow as a researcher with passion and desire for study. Also, I learned how to be a good leader from him.

Next, I like to express my gratitude to examining committee members, Prof. Tae-Hyuk Kwon and Prof. Jeong Kon Seo as well as collaborator for my research. They gave me a lot of helpful comments and kind advices. I also want to show appreciation to Prof. Hyunwoo Rhee who is now in Seoul National University for equipment support without any credit. If there was no support from him and his lab members, I could not produce experimental outcomes.

When it comes to my graduate school life, Kee lab members (Hoyoung, Juyoung, Ji-Young, Sun Hye, Seungmin, and Donghee) have given me the best supports. They were my advisers, coworkers, and friends. Especially, I want to give my biggest thanks to my teammates Hoyoung and Sun Hye. Even though they are not in our lab now, I do not forget my former teammates Ohyeon, Choong Keun, Hak-Jin, Ji Won, and Gwangsu.

Lastly, I really want to say "thank you" to my family for their unconditional love and support, as well as my best friends Taehoon and Gyuyeon. When I was tired out during the lab life, I sometimes go home and meet my family and friends. Maybe it seems trivial, but it had filled me energy to make a step forward. Thanks to all of you.